AD-A055 260 PENNSYLVANIA STATE UNIV UNIVERSITY PARK APPLIED RESE--ETC F/G 13/10
INITIAL INVESTIGATION OF STATIONARY HYDROFOIL CAVITATION AND CA--ETC(U)
DEC 77 D E THOMPSON, M L BILLET N00017-73-C-1418
UNCLASSIFIED TM-77-327 NL

1 OF 1
AD
A055 260

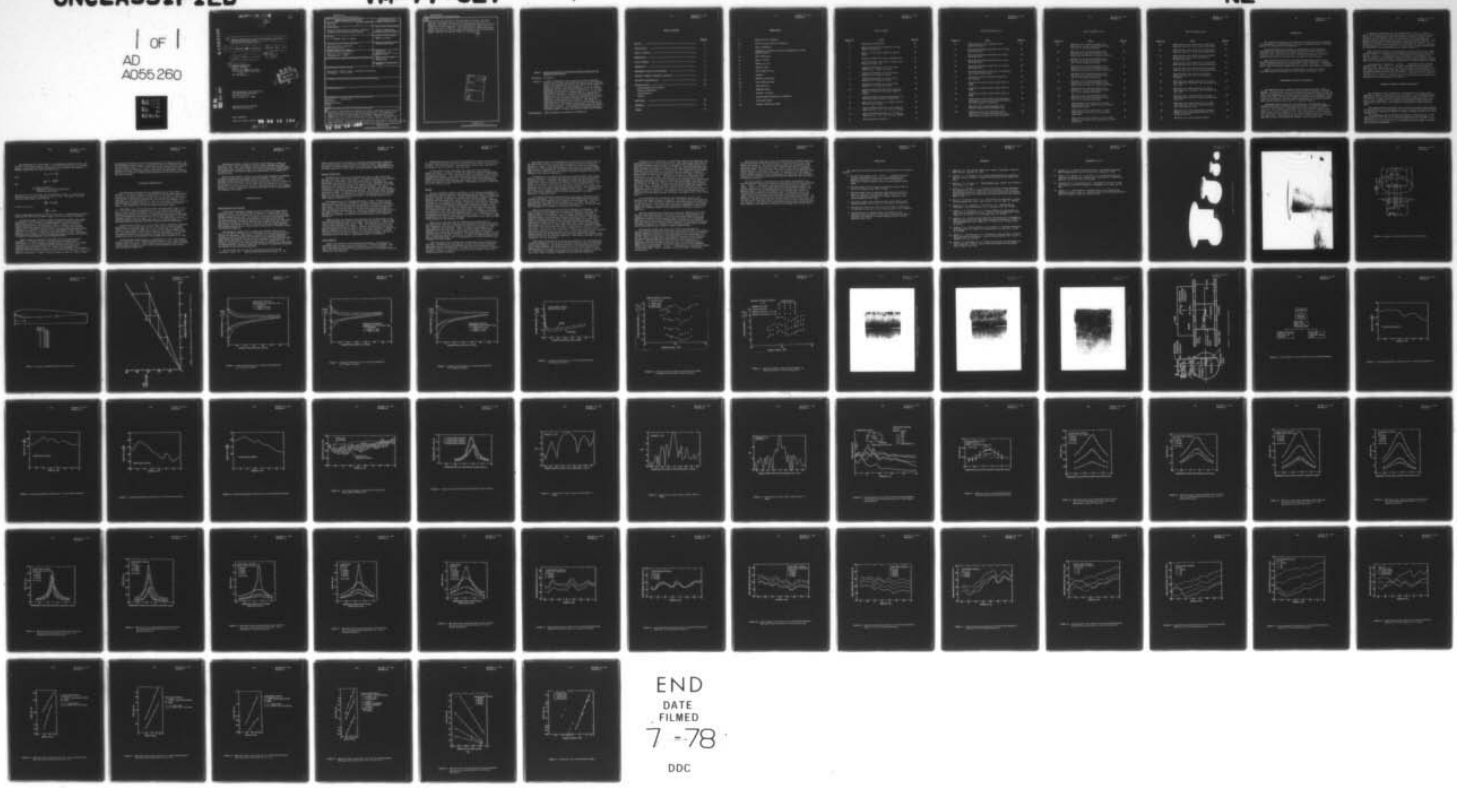

END
DATE
FILMED
7-78
DDC

12

(6) INITIAL INVESTIGATION OF STATIONARY HYDROFOIL CAVITATION AND CAVITATION NOISE SCALING

(10) D. E. Thompson M. L. Billet

(11) 16 Dec 77

(12) 74 P.

(14) TM-77-327

(9) Technical Memorandum
File No. TM 77-327
December 16, 1977
Contract No. N00017-73-C-1418

Copy No. (15) 64

The Pennsylvania State University
APPLIED RESEARCH LABORATORY
Post Office Box 30
State College, PA 16801

Approved for Public Release
Distribution Unlimited

NAVY DEPARTMENT

NAVAL SEA SYSTEMS COMMAND

UNCLASSIFIED

SECURITY CLASSIFICATION OF THIS PAGE (When Data Entered)

REPORT DOCUMENTATION PAGE		READ INSTRUCTIONS BEFORE COMPLETING FORM
1. REPORT NUMBER TM 77-327	2. GOVT ACCESSION NO.	3. RECIPIENT'S CATALOG NUMBER
4. TITLE (and Subtitle) INITIAL INVESTIGATION OF STATIONARY HYDROFOIL CAVITATION AND CAVITATION NOISE SCALING		5. TYPE OF REPORT & PERIOD COVERED Technical Memorandum 6. PERFORMING ORG. REPORT NUMBER
7. AUTHOR(s) D. E. Thompson and M. L. Billet		8. CONTRACT OR GRANT NUMBER(s) N00017-73-C-1418
9. PERFORMING ORGANIZATION NAME AND ADDRESS Applied Research Laboratory Post Office Box 30 State College, PA 16801		10. PROGRAM ELEMENT, PROJECT, TASK AREA & WORK UNIT NUMBERS
11. CONTROLLING OFFICE NAME AND ADDRESS Naval Sea Systems Command Washington, DC 20362		12. REPORT DATE December 16, 1977 13. NUMBER OF PAGES 71
14. MONITORING AGENCY NAME & ADDRESS(if different from Controlling Office)		15. SECURITY CLASS. (of this report) UNCLASSIFIED 15a. DECLASSIFICATION/DOWNGRADING SCHEDULE

16. DISTRIBUTION STATEMENT (of this Report)

Approved for public release. Distribution unlimited.
Per NAVSEA - May 26, 1978.

17. DISTRIBUTION STATEMENT (of the abstract entered in Block 20, if different from Report)

18. SUPPLEMENTARY NOTES

19. KEY WORDS (Continue on reverse side if necessary and identify by block number)

hydrofoils
cavitation
sheet cavitation
noise
scaling laws

20. ABSTRACT (Continue on reverse side if necessary and identify by block number)

A series of experiments were conducted in order to determine scaling laws for sheet type surface cavitation and the resulting noise. Four geometrically similar 10.6 percent thick symmetrical Joukowski hydrofoils with chord lengths of 1.5, 3, 6, and 12 inches were tested. Pressure distributions on the two largest hydrofoils were measured at several angles of attack. All noise measurements were made at an attack angle of 7° to produce the desired sheet cavitation. Desinent cavitation numbers were obtained as a function of →

DD FORM 1 JAN 73 1473 EDITION OF 1 NOV 65 IS OBSOLETE

78 06 12 186

UNCLASSIFIED

SECURITY CLASSIFICATION OF THIS PAGE (When Data Entered)

20. velocity for each hydrofoil at several angles of attack. The noise resulting from various amounts of cavitation on each hydrofoil was measured. The amount of cavitation was determined by the ratio of cavity length (L) to chord length (c). The relative cavity length (L/c) was varied from zero to one-third. Noise measurements included directivity patterns and spectra. The variation of cavitation noise with cavitation number, velocity, and Reynolds number was determined.

Subject: Initial Investigation of Stationary Hydrofoil Cavitation and Cavitation Noise Scaling

References: See Page 19

Abstract: A series of experiments were conducted in order to determine scaling laws for sheet type surface cavitation and the resulting noise. Four geometrically similar 10.6 percent thick symmetrical Joukowski hydrofoils with chord lengths of 1.5, 3, 6, and 12 inches were tested. Pressure distributions on the two largest hydrofoils were measured at several angles of attack. All noise measurements were made at an attack angle of 7^{o} to produce the desired sheet cavitation. Desinent cavitation numbers were obtained as a function of velocity for each hydrofoil at several angles of attack. The noise resulting from various amounts of cavitation on each hydrofoil was measured. The amount of cavitation was determined by the ratio of cavity length (L) to chord length (C). The relative cavity length (L/C) was varied from zero to one-third. Noise measurements included directivity patterns and spectra. The variation of cavitation noise with cavitation number, velocity, and Reynolds number was determined.

Acknowledgment: This investigation was sponsored by NAVSEA 03.

TABLE OF CONTENTS

	Page No.
Abstract	1
Acknowledgment	1
TABLE OF CONTENTS	2
NOMENCLATURE	3
LIST OF FIGURES	4
INTRODUCTION	8
EXPERIMENTAL FACILITY AND APPARATUS	8
HYDROFOIL CHORDWISE PRESSURE DISTRIBUTION	9
CAVITATION CHARACTERISTICS	11
CAVITATION NOISE	12
Data Acquisition and Analysis	
Acoustic Calibration	
Tests Conducted	
Results	
CONCLUSIONS	18
REFERENCES	19
FIGURES	21

NOMENCLATURE

A	aspect ratio of hydrofoil
A_e	effective aspect ratio of hydrofoil
b	span of hydrofoil
h	dimension of hydrofoil end plate perpendicular to mean velocity vector
C_L	lift coefficient
α	angle of attack
ρ	density of fluid
C	speed of sound
V	free stream velocity
P	pressure
C_P	pressure coefficient
P_∞	free stream pressure
P_V	vapor pressure
c	hydrofoil chord
ν	kinematic viscosity
L	cavity length along chord of hydrofoil
σ	cavitation number
σ_d	desinent cavitation number

LIST OF FIGURES

Figure No.	Title	Page No.
1	Photograph of Hydrofoils.	21
2	Typical Installation of Hydrofoil in Water Tunnel Test Section.	22
3	Sketch of 6-inch Chord Hydrofoil with End Plate.	23
4	Location of Hydrofoil Surface Pressure Taps.	24
5	Lift Coefficient versus Angle of Attack with Slopes of 2π and 1.2π.	25
6	Pressure Distribution for 12-inch Chord Hydrofoil at 7^{o} Angle of Attack.	26
7	Pressure Distribution for 12-inch Chord Hydrofoil at 5^{o} Angle of Attack.	27
8	Pressure Distribution for 6-inch Chord Hydrofoil at 7^{o} Angle of Attack.	28
9	Pressure Distribution for 12-inch Chord Hydrofoil at 0^{o} Angle of Attack.	29
10	Desinent Cavitation Number versus Reynolds Number for Hydrofoils at Various Angles of Attack.	30
11	Cavitation Number versus Reynolds Number for Various Cavitation States on Hydrofoils.	31
12	Spotty Type Cavitation at 7^{o} Angle of Attack. ($C = 12"$, $V_{\infty} = 45fps$)	32
13	Typical Developed Cavitation at 7^{o} Angle of Attack for $L/C = 1/6$. ($C = 12"$, $V_{\infty} = 45fps$)	33
14	Typical Developed Cavitation at 7^{o} Angle of Attack for $L/C = 1/3$. ($C = 12"$, $V_{\infty} = 45fps$)	34
15	Noise Measurement Apparatus.	35

LIST OF FIGURES (con't)

Figure No.	Title	Page No.
16	Block Diagram of Data Acquisition and Analysis Equipment.	36
17	Receiving Hydrophone Sensitivity for 1.5-inch Chord Hydrofoil.	37
18	Receiving Hydrophone Sensitivity for 3-inch Chord Hydrofoil.	38
19	Receiving Hydrophone Sensitivity for 6-inch Chord Hydrofoil.	39
20	Receiving Hydrophone Sensitivity for 12-inch Chord Hydrofoil.	40
21	Receiving Hydrophone Sensitivity in Free-Field and in Water Tunnel Setup.	41
22	Directivity with Each Hydrofoil Mounted in Test Section.	42
23	Directivity in Water Tunnel without Model ac 15kHz.	43
24	Directivity in Water Tunnel without Model at 35kHz.	44
25	Directivity in Water Tunnel without Model at 50kHz.	45
26	Sound Pressure Level Spectra with Receiving Hydrophone at Various Axial Positions Relative to a Fixed Amount of Cavitation.	46
27	RMS Noise Level versus Hydrophone Axial Position Depicting Noise Repeatability.	47
28	RMS Noise Level versus Hydrophone Axial Position for 1.5-inch Chord Hydrofoil with Spotty Type Cavitation at Various Velocities.	48

LIST OF FIGURES (con't)

Figure No.	Title	Page No.
29	RMS Noise Level versus Hydrophone Axial Position for 1.5-inch Chord Hydrofoil with L/C = 1/3 at Various Velocities.	49
30	RMS Noise Level versus Hydrophone Axial Position for 3-inch Chord Hydrofoil with Spotty Type Cavitation at Various Velocities.	50
31	RMS Noise Level versus Hydrophone Axial Position for 3-inch Chord Hydrofoil with L/C = 1/3 at Various Velocities.	51
32	RMS Noise Level versus Hydrophone Axial Position for 6-inch Chord Hydrofoil with Spotty Type Cavitation at Various Velocities.	52
33	RMS Noise Level versus Hydrophone Axial Position for 6-inch Chord Hydrofoil with L/C = 1/3 at Various Velocities.	53
34	RMS Noise Level versus Hydrophone Axial Position for 12-inch Chord Hydrofoil with Spotty Type Cavitation at Various Velocities.	54
35	RMS Noise Level versus Hydrophone Axial Position for 12-inch Chord Hydrofoil with L/C = 1/6 at Various Velocities.	55
36	RMS Noise Level versus Hydrophone Axial Position for 12-inch Chord Hydrofoil with L/C = 1/3 at Various Velocities.	56
37	Sound Pressure Level Spectra for 1.5-inch Chord Hydrofoil with Spotty Type Cavitation at Various Velocities.	57
38	Sound Pressure Level Spectra for 1.5-inch Chord Hydrofoil with L/C = 1/3 at Various Velocities.	58
39	Sound Pressure Level Spectra for 3-inch Chord Hydrofoil with Spotty Type Cavitation at Various Velocities.	59

LIST OF FIGURES (con't)

Figure No.	Title	Page No.
40	Sound Pressure Level Spectra for 3-inch Chord Hydrofoil with L/C = 1/3 at Various Velocities.	60
41	Sound Pressure Level Spectra for 6-inch Chord Hydrofoil with L/C = 1/3 at Various Velocities.	61
42	Sound Pressure Level Spectra for 12-inch Chord Hydrofoil with Spotty Type Cavitation at Various Velocities.	62
43	Sound Pressure Level Spectra for 12-inch Chord Hydrofoil with L/C = 1/6 at Various Velocities.	63
44	Sound Pressure Level Spectra for 12-inch Chord Hydrofoil with L/C = 1/3 at Various Velocities.	64
45	Sound Pressure Level Spectra for Various Hydrofoils with L/C = 1/3 at a Velocity of 35 ft/sec.	65
46	RMS Noise Level versus Velocity for 1.5-inch Chord Hydrofoil with Spotty Type Cavitation and L/C = 1/3.	66
47	RMS Noise Level versus Velocity for 3-inch Chord Hydrofoil with Spotty Type Cavitation and L/C = 1/3.	67
48	RMS Noise Level versus Velocity for 6-inch Chord Hydrofoil with Spotty Type Cavitation and L/C = 1/3.	68
49	RMS Noise Level versus Velocity for 12-inch Chord Hydrofoil with Spotty Type Cavitation, L/C = 1/6, and L/C = 1/3.	69
50	RMS Noise Level versus Normalized Cavitation Number for the 12-inch Chord Hydrofoil with Various Velocities.	70
51	RMS Noise Level versus Reynolds Number.	71

INTRODUCTION

The analytical treatment of the noise due to cavitation is very difficult. As a consequence, rational experiments designed to understand some of the basic aspects of cavitation noise are desirable.

The present memorandum considers an experimental program designed to investigate some basic aspects of sheet type surface cavitation and the resulting noise. Emphasis in the present investigation is on the scaling of cavitation noise with cavitation number, velocity, and hydrofoil size. A geometrically similar set of hydrofoils was employed in the program.

Each hydrofoil was tested in the 48-inch diameter Water Tunnel at the Applied Research Laboratory of The Pennsylvania State University. The noise spectra and directivities were measured for surface cavitation occurring over a range of cavitation numbers and velocities for each hydrofoil considered.

Based on the results obtained, considerations are given to scaling cavitation noise with velocity, cavitation number, and hydrofoil size.

EXPERIMENTAL FACILITY AND APPARATUS

The experiments were conducted in the 48-inch diameter Water Tunnel of ARL/PSU. The test section is 14 feet long and 4 feet in diameter. The water velocity in the bare test section can be varied continuously from 0 to about 60 ft/sec and, independently, the test section pressure can be continuously varied from 6 to 40 psia. The total air content of the water can be reduced to about 2 ppm on a mole basis. For more detailed information on the 48-inch diameter water tunnel characteristics, refer to a report by Lehman (1).

Experiments were conducted on four hydrofoils. The hydrofoils were geometrically similar in planform and cross-section, and had chord lengths of 1.5, 3, 6, and 12 inches. A photograph of the four hydrofoils is shown in Figure 1. In order to maintain similar flow fields for each hydrofoil, the aspect ratio was held constant at 0.66. The cross-section of each hydrofoil was a modified Joukowski airfoil section with a maximum thickness of 10.6% of the chord length. The modification consisted of replacing the cusped trailing edge with a linear distribution for reasons of ease of manufacture.

A directional hydrophone was used to measure the surface cavitation noise. Its focal point was on the centerline of the water tunnel test section. Therefore, the cavitating region of each hydrofoil had to be located in the center of the test section. Since the aspect ratio of the hydrofoils was constant and the chords changed, the span of each hydrofoil was different. Each hydrofoil was mounted on a flat plate which spanned the test section. The location of the flat plate was different for each hydrofoil such that the center of the hydrofoil was in the center of the test section. A typical installation as illustrated by the 12-inch hydrofoil is shown in Figure 2.

When a hydrofoil operates on a flat plate as shown in Figure 2, the inflow to the hydrofoil is influenced by the boundary layer formed on the flat plate and the surface cavitation will be influenced by this boundary layer. So that the influence of the boundary layer is the same for each hydrofoil, the ratio of boundary layer thickness to hydrofoil span was made constant by placing each foil at an appropriate distance downstream of the leading edge of the plate.

It was desired to investigate surface cavitation and the resulting radiated sound. The surface cavitation was generated by operating the hydrofoils at an appropriate angle of attack. In order to avoid formation of a tip vortex cavity at the same time that a blade surface cavity was present, an end plate was added to the tip of each hydrofoil. The end plates were designed to produce no lift. Each end plate was sized to be consistent with the hydrofoil upon which it was mounted. A typical hydrofoil with end plate is illustrated by the sketch of the 6-inch hydrofoil in Figure 3.

HYDROFOIL CHORDWISE PRESSURE DISTRIBUTION

The chordwise pressure distribution was measured for the 12-inch chord hydrofoil at angles of attack of 0°, $\pm 3^{\circ}$, $\pm 5^{\circ}$, and $\pm 7^{\circ}$. The chordwise pressure distribution for the 6-inch hydrofoil was measured at angles of attack of $\pm 3^{\circ}$, $\pm 5^{\circ}$, and $\pm 7^{\circ}$. Figure 4 shows the location of the pressure taps used in this part of the investigation. The chordwise distribution of pressure taps was established so that one tap was located at the theoretical minimum pressure point.

The Douglas-Neumann program was used to compute the pressure distributions for the hydrofoils at various angles of attack. The particular program employed was based on an extension to problems of lifting, infinite cascades as developed by Giesing (2).

The assumptions used in deriving the analytical technique do not, in all cases, match the real flow of the hydrofoils employed in the experiment. In particular, the flow is assumed to be two-dimensional in the analysis, whereas, the end plate and low aspect ratio of the hydrofoils tested result in the real flow being three-dimensional.

The theoretical lift curve slope of a two-dimensional hydrofoil is 2π. The effects of the end plate and low aspect ratio can be accounted for in the following way. As discussed in Doerner and Borst (3), the end plate will induce an effective aspect ratio for the hydrofoil given by

$$A_e = A \left[1 + \frac{\Delta A}{A}\right]$$

where

$$\frac{A}{\Delta A} = \left[1 - \left(\frac{b}{h}\right)^{\frac{4}{3}}\right]^{\frac{3}{4}}$$

and

b = span of hydrofoil
h = dimension of end plate perpendicular to mean velocity vector.

The ratio of b to h is the same for all hydrofoils tested, i.e. 0.88, and the effective aspect ratio is calculated to be $A_e = 3.47$. The slope of the lift curve for finite aspect ratio foils is

$$\frac{\partial C_L}{\partial \alpha} = 2\pi \frac{A}{A + 2}$$

or for $A = A_e = 3.47$

$$\frac{\partial C_L}{\partial \alpha} = 1.27\pi.$$

This is considerably different from the 2π value for a two-dimensional hydrofoil. A plot of the lift curve is shown in Figure 5 for the two slopes considered.

An effective angle of attack at which the hydrofoils operate can be found from Figure 5. For instance, at 7° geometric angle of attack the effective angle of attack is 4.4°. These effective angles of attack are used in correlating experimental and theoretical results. Consider, for instance, Figure 6 which shows pressure distributions for the 12-inch chord hydrofoil operating at a 7° geometric angle of attack. The experimental minimum pressure coefficient is seen to be -1.91 while the Douglas-Neumann program for the hydrofoil at 7° predicts a minimum pressure coefficient of -3.60. Employing an effective angle of attack of 4.5°, the predicted minimum pressure coefficient is -1.8 which is in good agreement with the measured value.

Figure 7 shows the pressure distributions for the 12-inch hydrofoil operating at a 5° angle of attack. The experimental minimum pressure coefficient is -1.35, the predicted minimum pressure coefficient at a 5° angle of attack is -2.2, and the predicted minimum pressure coefficient at an effective angle of attack of 3° is -1.1. Again, the experimental and theoretical minimum pressure coefficients are in good agreement, if an effective angle of attack is used in the theory. Similar results are obtained for the 6-inch hydrofoil operating at 7° angle of attack as shown in Figure 8. Figure 9 shows

the pressure distribution for the 12-inch hydrofoil at 0° angle of attack. The Douglas-Neumann program predicts a distribution which is consistently less than the experimental values. This is consistent with the values for other angles of attack as shown in Figures 6, 7, and 8. This particular difference could perhaps be ascribed to manufacturing inaccuracies of the hydrofoils. However, each foil was checked on a blade inspection machine and they were found to have the correct profile.

CAVITATION CHARACTERISTICS

The cavitation characteristics were determined for the four similar hydrofoils. As shown in Figure 10, the desinent cavitation number was obtained for most of the foils at angles of attack of 1°, 3°, 5°, and 7°. Because of tunnel pressure limitations, the 1.5-inch foil could not be tested at an angle less than 7°. This result determined that for the noise measurements, the operating angle of attack would be 7°. Also, the zero-degree reference line for each foil was determined by testing the foil for both positive and negative angles. This ensured that the true zero-degree setting was known.

From Figure 11, it can be seen that over a Reynolds number range of 3.3×10^5 to 5.4×10^6, which is approximately 16:1, the cavitation results do not show a uniform scaling relationship. Also, these results, which include variation with velocity and size, do not show trends as observed by Parkin and Holl (4) on hemispherical nosed bodies or by Holl and Wislicenus (5) on 12% thick Joukowski hydrofoils at zero angle of attack. On the other hand, a jump in cavitation number, which for these tests occurs at a Reynolds number of 7×10^5, has been observed by Robertson, McGinley and Holl (6) on 1/8 caliber noses.

From the work by Arakeri (7, 8, 9), Figure 11 can be explained by analyzing the boundary layer behavior over the foil. This jump in cavitation number, which occurs at a Reynolds number of 7×10^5, could be due to a transition between a long separation bubble, which occurs at low Reynolds numbers, and a short separation bubble, which occurs at high Reynolds numbers. As discussed in Huang and Peterson (10), the presence of a long separation bubble can significantly reduce the magnitude of the minimum static pressure of the body.

As the Reynolds number increases to approximately 2×10^6, there appears to be an elimination of the laminar separation bubble so that a fully turbulent boundary layer flow exists. Larger pressure fluctuations occur with transition of the separation bubble than with a fully turbulent boundary layer flow as shown by Huang and Hannan (11).

The Reynolds numbers at which the boundary layer appears to change for these tests will vary with parameters such as surface roughness and tunnel turbulence level. Also, this change in characteristic for the Joukowski foils over a large range of Reynolds numbers will lead to differences in the dynamics of bubble growth. This must be taken into consideration in the analysis of cavitation noise.

The cavitation numbers at which noise results were obtained are summarized in Figure 11 along with the desinent cavitation numbers. In all, three cavitation states were chosen which were [1.] spotty type cavitation, [2.] developed cavitation having a cavity length-to-chord ratio (L/C) of 1/6 (for the 12-inch hydrofoil only), and [3.] developed cavitation having an L/C of 1/3. Photographs of the cavitation for each test point were obtained. As an example, Figures 12, 13 and 14 show three cavitation conditions for the 12-inch hydrofoil at a velocity of 45 ft/sec.

CAVITATION NOISE

Data Acquisition and Analysis

A directional hydrophone assembly was used to measure the blade surface cavitation noise. The system is shown in Figure 15. A water filled tank is mounted to one side of the tunnel test section with the directional hydrophone assembly immersed in the tank. The reflector is the end of an ellipsoid with one focus of the ellipsoid on the centerline of the test section and the receiving hydrophone, an Atlantic Research LC-10, positioned at the other focus. The path of the sound is from the test section centerline, through the plexiglass window, and through the water in the tank to the receiving hydrophone. The plexiglass window has a ρc close to that of water and is, therefore, nearly acoustically transparent.

The hydrophone assembly can be continuously traversed along the test section, so that the directivity of a sound source on the test section centerline can be determined. This ability to traverse the receiving hydrophone assembly was used to determine the beam width of the receiving hydrophone. A known source was placed on the test section centerline and located in the axial center of the test section. With the source driven at a known level and frequency, the output of the receiving hydrophone was recorded at a large number of axial positions. Lauchle (12) describes, in detail, the calibration technique and results for the reflecting hydrophone.

The instrumentation for the data acquisition and analysis of the cavitation noise is shown in block diagram form in Figure 16. The

signal received from the hydrophone was amplified with an ARL built amplifier. It was then high and low pass filtered from 15kHz to 70kHz. This signal was analyzed on a Spectral Dynamics 301-C real time analyzer and simultaneously the root mean square value of the signal was measured with a DISA 55035 RMS meter.

Acoustic Calibration

Calibration of the receiving hydrophone was done for each of the foils mounted in the water tunnel test section. An Atlantic Research LC-10 hydrophone was used as a sound source. The noise sources, due to cavitation, are distributed over some part of the surface of each foil. Therefore, the sound source for calibration was placed at the midspan of each hydrofoil at the axial location of the cavitation collapse zone being investigated. For these configurations, the spectra of the received sound from the sound source being driven with a white noise voltage were obtained. The frequency range considered was from 0 to 50kHz. In addition with the sound source located in the mid-span plane for each foil, the directivity in terms of the RMS level of the received signal for the mid-span plane was determined in the frequency band of 15 to 70kHz along the hydrofoil chord.

The sensitivity of the receiving hydrophone, in situ, is shown for the different foils in Figures 17 through 20. As seen, there are some broadband humps in the sensitivity curves which are ascribed to resonances in the tunnel test section. This is supported by the sensitivity curve for the hydrophone with a sound source with no model in the test section as shown in Figure 21, which was obtained from Reference 12. Notice the broadband humps centered at 22 and 42kHz in Figure 12. The location of broadband humps in the spectra were modified by the presence of models in the test section as seen in Figures 17 through 20.

Figure 22 shows the results of the calibration of the directivity of the receiving hydrophone with each foil mounted in the test section. These are RMS levels in the frequency range of 15 to 70kHz. The directivity for the 1.5 and 3.0-inch chord hydrofoils are similar. Also, the directivity of the 6.0 and 12.0-inch chord hydrofoils are similar. However, the directivity for the two smaller hydrofoils is different than for the two larger hydrofoils. Lauchle (12) measured directivities with no model in the tunnel test section. His sound source was driven with each of a number of pure tones and typical results are reproduced here for the sake of completeness, Figures 23 through 25.

Tests Conducted

Based on the results of the cavitation investigation, measurements of cavitation noise were made with each hydrofoil at a 7° angle of attack. This particular angle of attack resulted in the desired type of cavitation, i.e. sheet, and the desired amount of developed cavitation over the velocity range of interest for each hydrofoil.

Measurements were made for each foil operating with spotty type cavitation. The spotty type cavitation condition is defined as the cavitation which exists at a pressure just below desinence. Measurements with spotty type cavitation at velocities of 30, 35, 45 and 55 ft/sec were made.

It was desired to also investigate the noise from fully developed surface cavitation. In order to obtain some similarity between the cavitation which exists from foil to foil, the ratio of area of cavitation to area of foil was maintained constant. The constant was chosen such that the ratio of cavity length-to-foil chord length was 1/3. For the foil with a chord length of 12 inches, an additional fully developed cavity with a ratio of cavity length-to-foil chord length of 1/6 was investigated. Measurements were made at velocities of 30, 35, 45 and 55 ft/sec.

Results

For each cavitation condition considered, it was desired to determine the directivity of radiated sound in a plane intersecting the hydrofoil midspan. It was desired to plot the RMS level, in some frequency band, versus the hydrophone position. However, in addition to the RMS level, spectral content of the radiated sound can change with relative location of the hydrophone. Therefore, the spectra of the radiated sound from a 2-inch long cavity on the 6-inch chord hydrofoil for the hydrophone at a number of positions were obtained. Figure 26 shows the spectra at representative hydrophone locations with respect to the hydrofoil leading edge. As seen, the spectra have essentially the same shape for frequencies above 15kHz. However, below 15kHz, the shape of the spectra are different for each different hydrophone position. In addition, below 5kHz the possibility exists that the background levels, i.e. no cavitation, may be contaminating the received signal with cavitation present. As a result of these observations, the levels in the directivity curves shown in this report are RMS values measured in the bandwidth 15-70kHz.

Exact size of the cavity and the chordwise and spanwise extent of cavitation do not repeat for identical test conditions of velocity and pressure. As a consequence, the level and spatial distribution of noise do not repeat for those identical test conditions. Figure 27 shows a typical example of the repeatability of the directivity curves. Each open symbol results from a separate test in which the reflecting hydrophone was scanned in discrete increments past the cavitating hydrofoil. At each hydrophone position, the RMS level of noise was recorded. As seen in the figure, the maximum spread in the data is approximately 6dB. This is representative of the data spread obtained throughout the test program.

With the large scatter involved, data interpretation and correlation was difficult. Therefore, for each hydrofoil at each test condition considered, many scans with the reflecting hydrophone were made and an average at each hydrophone position was determined. An example of the result of this procedure is shown in Figure 27, where the dark circles are the average level at each hydrophone position considered.

The average result of the measurements of directivity of noise for each of the hydrofoils at each of the cavitation conditions are shown in Figures 28 through 36. Each of these figures shows the RMS noise level, in a frequency band of 15 to 70kHz, versus the hydrophone position from the hydrofoil leading edge (positive is upstream) for the various test conditions considered. Each figure is for a hydrofoil with a particular cavitation condition, and shows the levels for each velocity considered.

As expected, as the velocity increases for a given hydrofoil with a given amount of cavitation, the noise level increases except for one case which will be discussed later. In general, the shapes of the various directivities are similar with a peak in level near the location of the collapsing portion of the cavity and a decrease in level in the upstream and downstream directions. It should be noted that as the cavity becomes longer, the peak in the level moves downstream since the cavity collapse zone moves downstream. This indicates that the noise, in the frequency range considered, from surface cavitation is due to the bubble collapse zone of the cavity as opposed to the bubble generation or transport zones.

It is easily noted that the directivity of the sound is different for the different hydrofoils. The 1.5-inch and 3-inch chord hydrofoils have similar directivities with beamwidths of 9.0 inches at the 3dB downpoints. The 6-inch chord hydrofoil has a much narrower beamwidth of 1.5 inches. The 12-inch hydrofoil has a beamwidth of 9.5 inches for velocities of 30, 35, and 45 ft/sec and a beamwidth of 1.5 inches for a velocity of 55 ft/sec.

There are two possible causes for these differences in beamwidth. The first is that the flow regimes over each foil are different, which cause the bubble dynamics of the cavitation to be different, and hence, the noise characteristics to be different. There is further evidence to support this contention based on the previsouly discussed cavitation results. Referring to Figure 11 showing cavitation number versus Reynols number, it was seen that there was no uniform behavior of the cavitation with Reynolds number. It was postulated in a previous section of this report that there are two different flow regimes, one for the 1.5 and 3-inch chord foils, a long separation bubble, and one for the 6 and 12-inch chord foils, a short bubble or possibly no separation bubble. This postulation is supported further by the cavitation noise directivity patterns, i.e. in general, the 1.5 and 3-inch chord foils have different directivity patterns compared to those of the 6 and 12-inch chord foils. Further support for this contention results from the shape of the spectra of the cavitation noise for the different hydrofoils. This will be discussed in detail subsequently in this memorandum.

These large differences in the directivity patterns of the cavitation noise cannot be explained in terms of the directivity related to foil size influences on the sound radiation. As discussed previously, the directivity for each foil with a known broadband sound source located at 1/3 the chord length from the leading edge and at midspan was determined and the results are shown in Figure 22. Essentially, the shapes of the directivity curves are similar for all four foils with a small increase in beamwidth for the larger two hydrofoils.

In addition to the directivity, representative spectra were obtained of the sound pressure level of the cavitation noise. Each spectrum was taken with the receiving hydrophone positioned where the maximum level occurred based on the directivity patterns shown in Figures 28 through 36. The resulting spectra are shown in Figures 37 through 44. Because of the repeatability problem discussed previously, the comparative levels for different test conditions are inaccurate since each spectrum is only one spectrum and not the average of a number of spectra taken at identical test conditions. However, the shape of the spectra are accurate. It is seen from the figures that for a consistent set of conditions involving foil size and cavity size, the spectral shape does not change with velocity, except for the 12-inch chord foil where at 30 and 35 ft/sec the shapes below 22kHz are similar to each other and different from those of 45 and 55 ft/sec. In addition, for each foil the spectral shape does not change with cavity size. One notes, however, that the spectral shape does change with foil size. Figure 45 shows this for a velocity of 35 ft/sec and a cavity length-to-foil size ratio of 1/3. The spectra for the 1.5 and 3-inch foils are similar in shape to each other. The spectra for the 6 and 12-inch foils are also similar to each other in shape, but differ from those of the 1.5 and 3-inch foils.

It is postulated that the spectral shape differences are due to the different flow regimes discussed previously. The shapes of the spectra for the 1.5 and 3-inch foils, for which a separated flow regime exists, are similar and the spectra for the 6 and 12-inch foils, for which a nonseparated flow regime exists, are similar. Since the bubble dynamics are different for the two flow regimes, the frequency content of the sound would be different, as shown in Figure 45.

Previous investigations of noise from cavitation, References (13), (14), and (15), have shown that there are peaks in the noise spectra which can be related to the bubble dynamics. In the investigations considered here, the spectra were obtained in the frequency range 15 to 50kHz, due to background limitations on the low end and instrumentation limitations on the high end. With this rather limited frequency range considered, no conclusions with regard to peaking of spectra or to scaling of the resulting spectra could be reached. Future investigations will consider a larger frequency range.

The variation of RMS noise level with velocity was determined by crossplotting from Figures 28 through 36 the peak levels of noise. The results, shown in Figures 46 through 49, are plotted as RMS noise level versus velocity. The RMS noise level was found to vary approximately as the second power of velocity, hence, the mean square level varies as velocity to the fourth power for all cavitation conditions on all hydrofoils except the 1.5-inch chord hydrofoil. The variation with velocity for the 1.5-inch hydrofoil is approximately 0.9 for developed cavitation and 3.0 for limited cavitation. Blake, et al (13) has observed that the mean square level of both separation induced and traveling bubble surface cavitation noise increased as velocity to the fourth power. This is consistent with the findings of the present investigation.

The variation of RMS noise level with nondimensional cavitation number was determined for the 12-inch chord hydrofoil at the peak levels of noise from Figures 34 through 36. The results, shown in Figure 50, are plotted as RMS noise level versus the cavitation number nondimensionalized by the desinent cavitation number. Four curves are shown, one for each velocity considered, each of which has a different slope. As seen, the slope of the RMS noise level becomes steeper as the velocity increases. It appears that for the range of test conditions employed in this investigation, the RMS noise level increases linearly with decreasing nondimensional cavitation number and that the slope is a function of velocity.

As noted previously, one objective of the present investigation is to determine scaling laws for blade surface cavitation and for the noise resulting from surface cavitation. One possible scaling parameter is Reynolds number. Figure 51 is a plot of RMS noise level versus Reynolds number. One can see that there is no consistent behavior of the RMS level of noise with Reynolds number. This can be ascribed to the postulation that there are different flow regimes for the different foils. As discussed, the 1.5 and 3-inch foils have a separated flow field whose extent varies with Reynolds number and the 6 and 12-inch foils do not have a separated region of flow. The behavior of the RMS noise level with Reynolds number follows a consistent curve for the 6 and 12-inch foils while the results for the 1.5 and 3-inch foils are not consistent. The results of the trend with Reynolds number of the RMS noise level supports the postulation of different flow regimes for different foils.

CONCLUSIONS

The conclusions derived from the present investigation can be listed as follows:

1. The cavitation number of the surface cavitation observed in this investigation does not scale systematically with Reynolds number based on foil size. This is postulated as being due to laminar separation over a certain Reynolds number range.

2. The mean square level of sheet type cavitation noise scales as V^4 in the frequency range 15kHz to 50kHz.

3. The mean square level of sheet type cavitation noise does not scale systematically with Reynolds number based on foil size This is postulated as being due to laminar separation over a certain Reynolds number range.

4. The level of sheet type cavitation noise scales linearly with cavitation number and the slope is a function of the velocity.

5. The noise for sheet type cavitation in the 15kHz to 50kHz range is believed to originate in the collapse region of the cavitation.

6. The distribution of spectral energy is different for the different foils considered in the present investigation. This is postulated as being due to laminar separation over a certain Reynolds number range.

REFERENCES

1. Lehman, A. F., "The Garfield Thomas Water Tunnel," ORL Report, Serial No. NOrd 16597-56, September 30, 1959.

2. Giesing, J. P., "Extension of the Douglas-Neumann Program to Problems of Lifting, Infinite Cascades," Douglas Aircraft Report No. LB 31653, July, 1964.

3. Hoerner, S. F. and Borst, H., "Fluid-Dynamic Lift," Hoerner Fluid Dynamics, Brick Town, N.J., 1975.

4. Parkin, B. R. and Holl, J. W., "Incipient Cavitation Scaling Experiments for Hemispherical and 1.5 Caliber Ogive-Nosed Bodies," A Joint Study by Hydrodynamics Laboratory, California Institute of Technology and Ordnance Research Laboratory, The Pennsylvania State University, No. NOrd 7958.264, May 15, 1953.

5. Holl, J. W. and Wislicenus, G. F., "Scale Effects on Cavitation," Journal of Basic Engineering, Trans. ASME, Series D, Vol. 83, 1961, pp. 385-398.

6. Robertson, J. M., McGinley, J. H. and Holl, J. W., "Similitude and Cavitation," La Houille Blanche, No. 4, September 1957, pp. 540-554.

7. Arakeri, V. H. and Acosta, A. J., "Viscous Effects in the Inception of Cavitation on Axisymmetric Bodies," Journal of Fluids Engineering, Trans. ASME, Vol. 95, Series 1, No. 4, December 1973, pp. 519-527.

8. Arakeri, V. H., "A Note on the Transition Observations on an Axisymmetric Body and Some Related Fluctuating Wall Pressure Measurements," Journal of Fluids Engineering, Trans. ASME, Vol. 97, Series 1, No. 1, March 1975, pp. 82-86.

9. Arakeri, V. H., "Viscous Effects on the Position of Cavitation Separation from Smooth Bodies," Journal of Fluid Mechanics, Vol. 68, Part 4, 1975, pp. 779-799.

10. Huang, T. T. and Peterson, F. B., "Influence of Viscous Effects on Model/Full-Scale Cavitation Scaling," Journal of Ship Research, Vol. 20, No. 4, December 1976, pp. 215-223.

11. Huang, T. T. and Hannan, D. E., "Pressure Fluctuations in the Regions of Flow Transition," David W. Taylor Naval Ship Research and Development Center, Report 4723, 1976.

REFERENCES (con't)

12. Lauchle, G. C., "Acoustic Characteristics of the ARL/FEU Ellipsoidal Reflecting Hydrophone," ARL TN 76-15 (Uncl), February 3, 1976.

13. Blake, W. K., Wolpert, M. J. and Geib, F. E., "Cavitation Noise and Inception as Influenced by Boundary Layer Development on a Hydrofoil," JFM, Vol. 80, May 20, 1977, pp. 617-640.

14. Fitzpatrick, H. M. and Strasberg, M., "Hydrodynamic Sources of Sound," 2nd Symposium on Naval Hydrodynamics, Washington, D.C., 1956, pp. 241-280.

15. Barker, S. J., "Measurements of Radiated Noise in the Caltech High-Speed Water Tunnel, Part II: Radiated Noise from Cavitating Hydrofoils," GAL/CIT, Pasadena, California, March 20, 1975.

FIGURE 1 - Photograph of Hydrofoils.

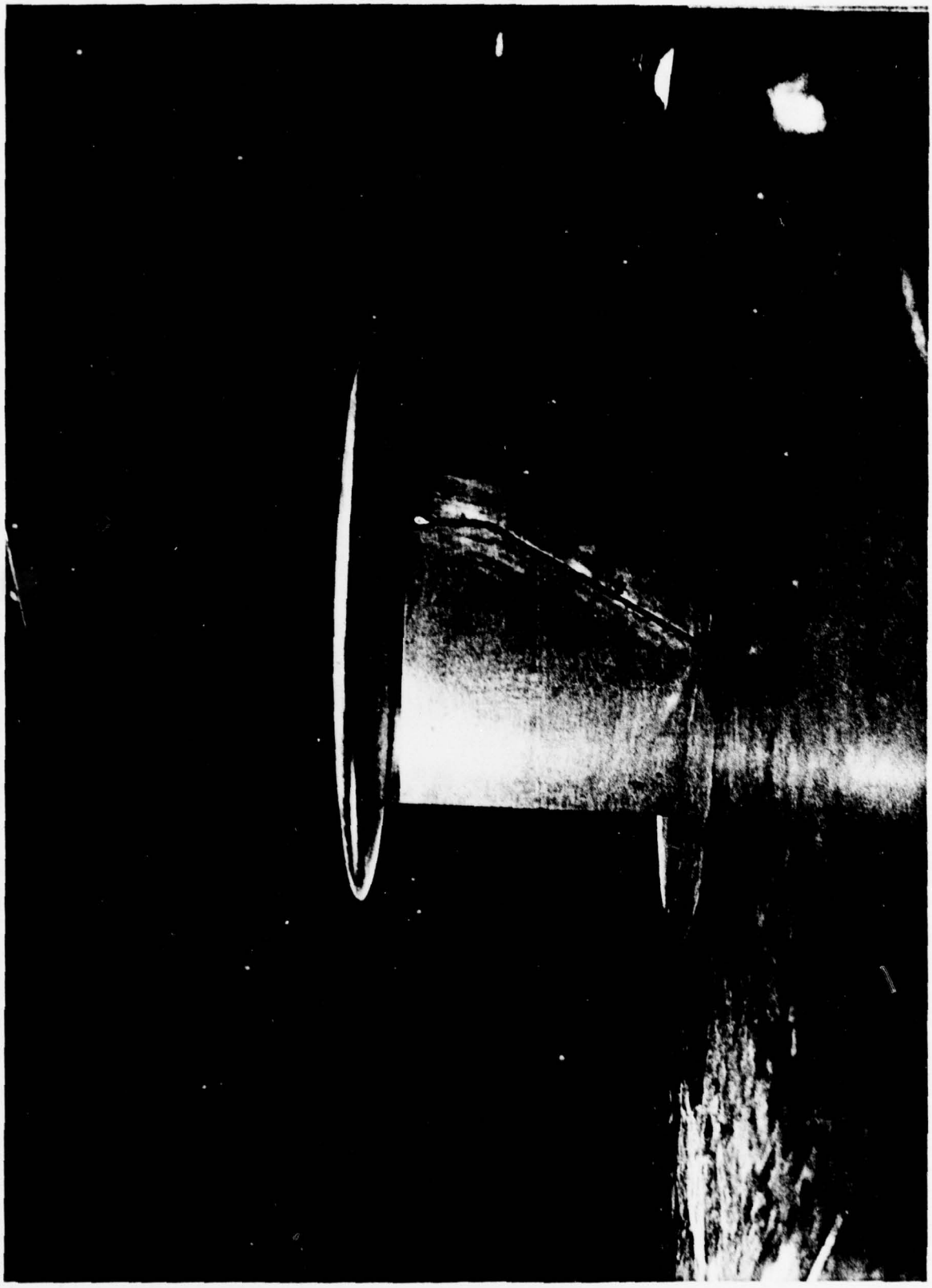

FIGURE 2 - Typical Installation of Hydrofoil in Water Tunnel Test Section.

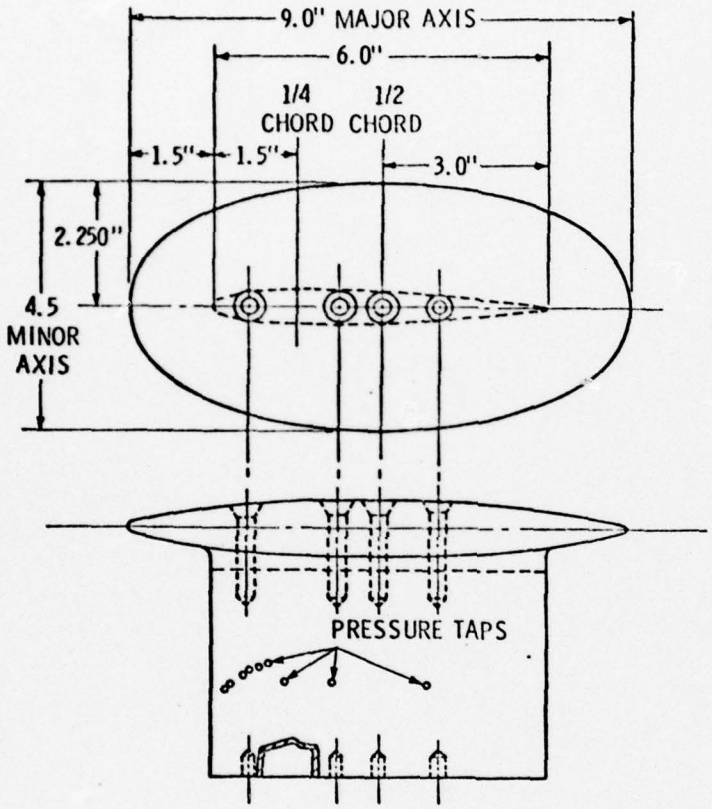

FIGURE 3 - Sketch of 6-inch Chord Hydrofoil with End Plate.

December 16, 1977
DET;MLB:sk

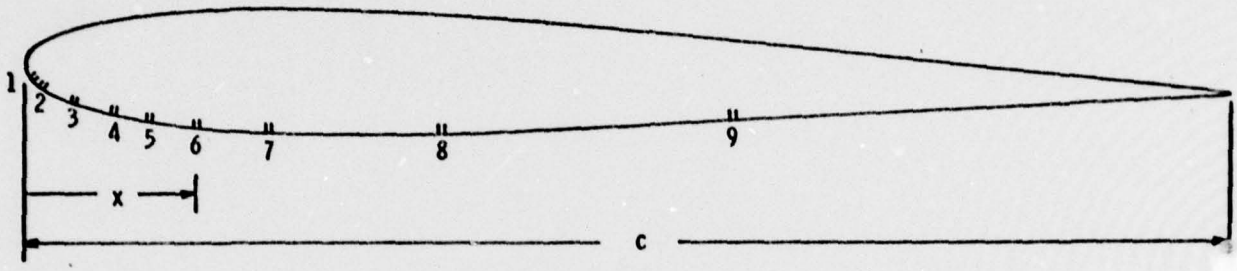

PRESSURE TAP No.	x/c
1	0.006
2	0.013
3	0.042
4	0.075
5	0.104
6	0.145
7	0.206
8	0.350
9	0.588

FIGURE 4 - Location of Hydrofoil Surface Pressure Taps.

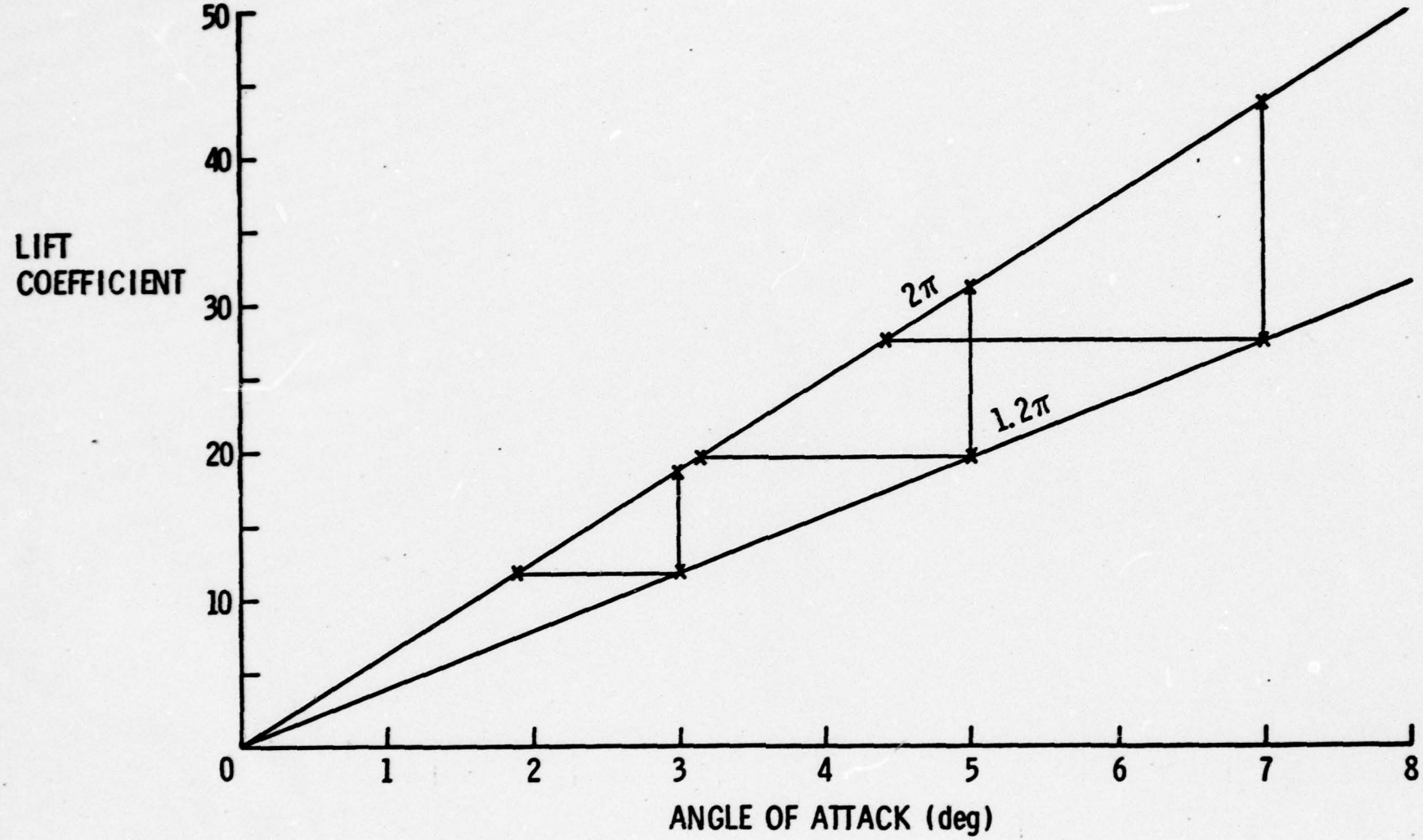

FIGURE 5 - Lift Coefficient versus Angle of Attack with Slopes of 2π and 1.2π.

December 16, 1977
DET:MLB:sk

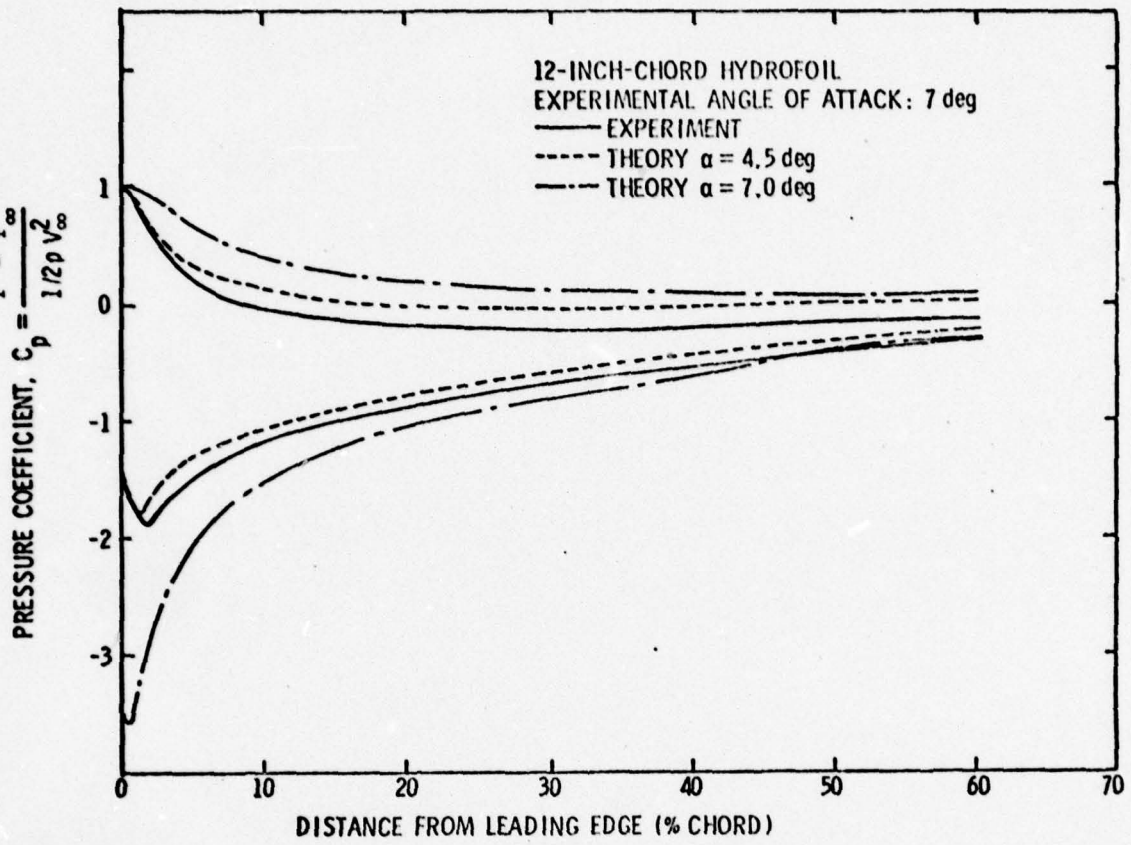

FIGURE 6 - Pressure Distribution for 12-inch Chord Hydrofoil at 7° Angle of Attack.

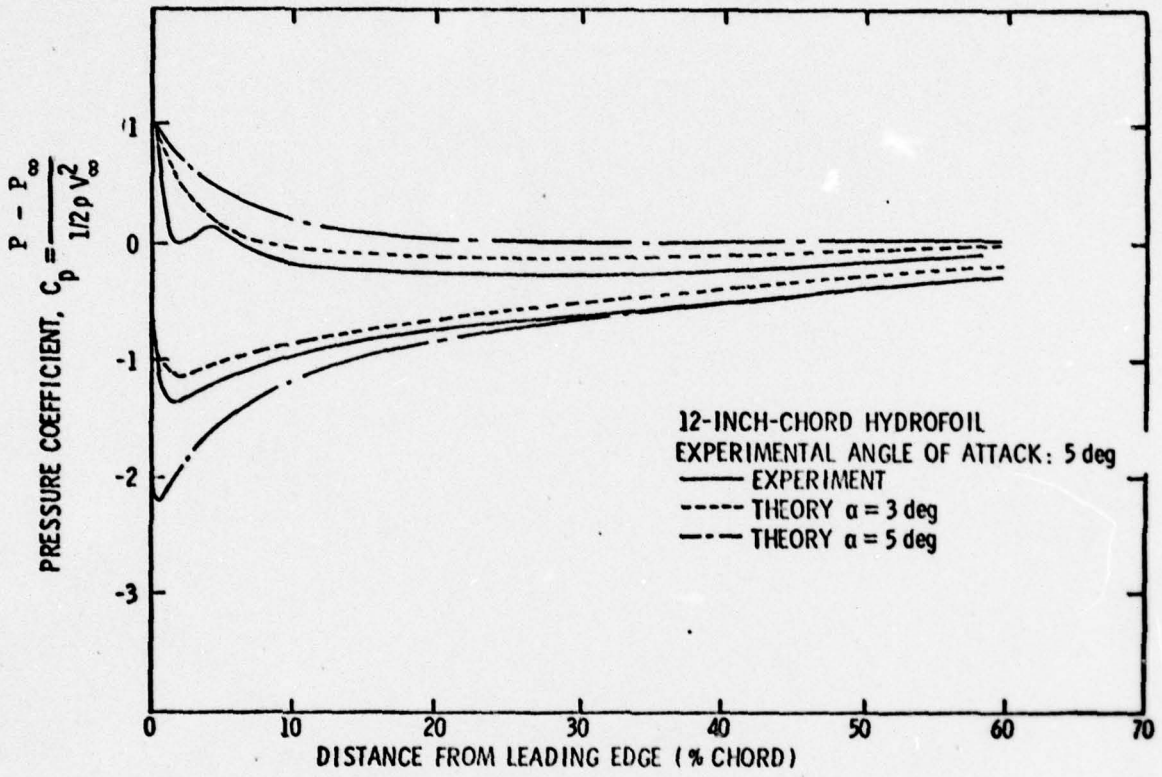

FIGURE 7 - Pressure Distribution for 12-inch Chord Hydrofoil at 5^{o} Angle of Attack.

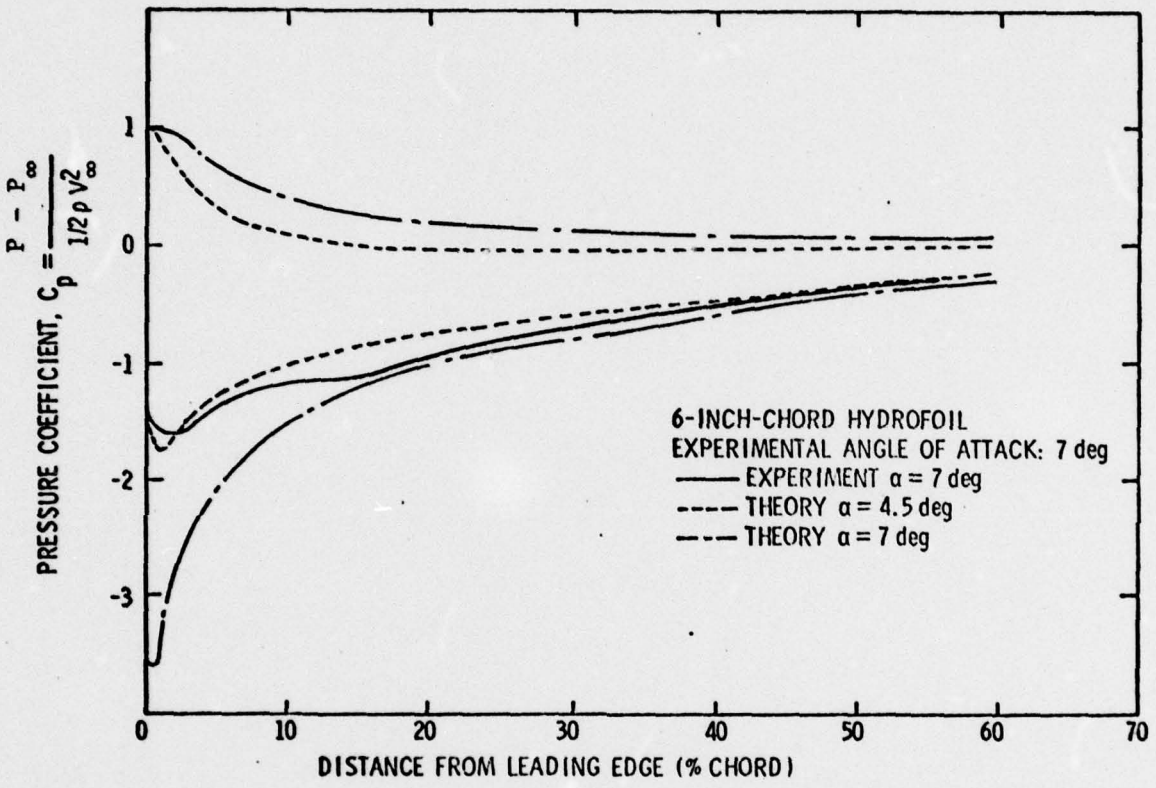

FIGURE 8 - Pressure Distribution for 6-inch Chord Hydrofoil at 7° Angle of Attack.

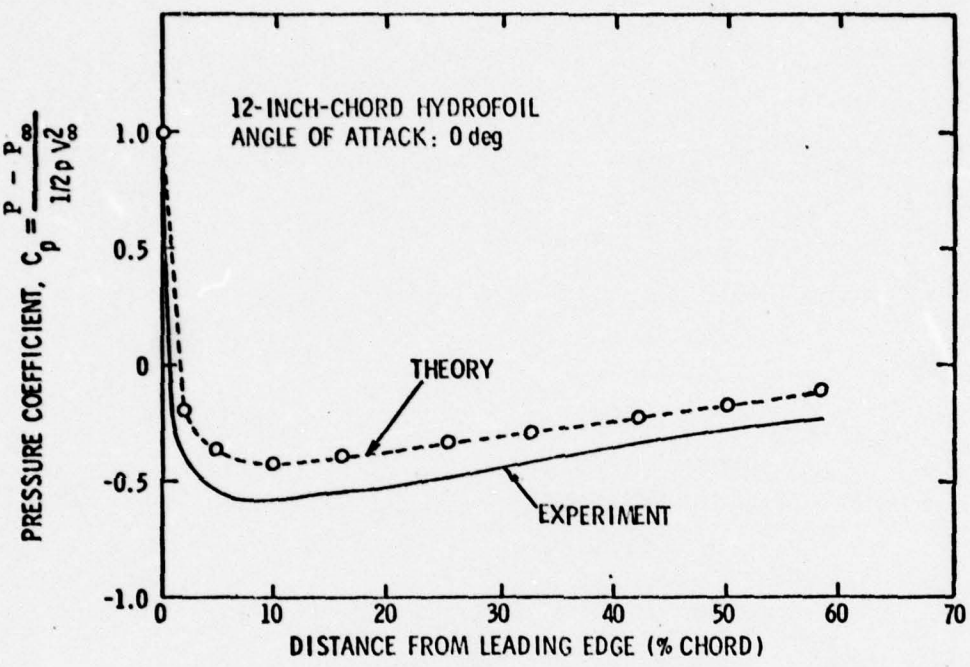

FIGURE 9 - Pressure Distribution for 12-inch Chord Hydrofoil at 0° Angle of Attack.

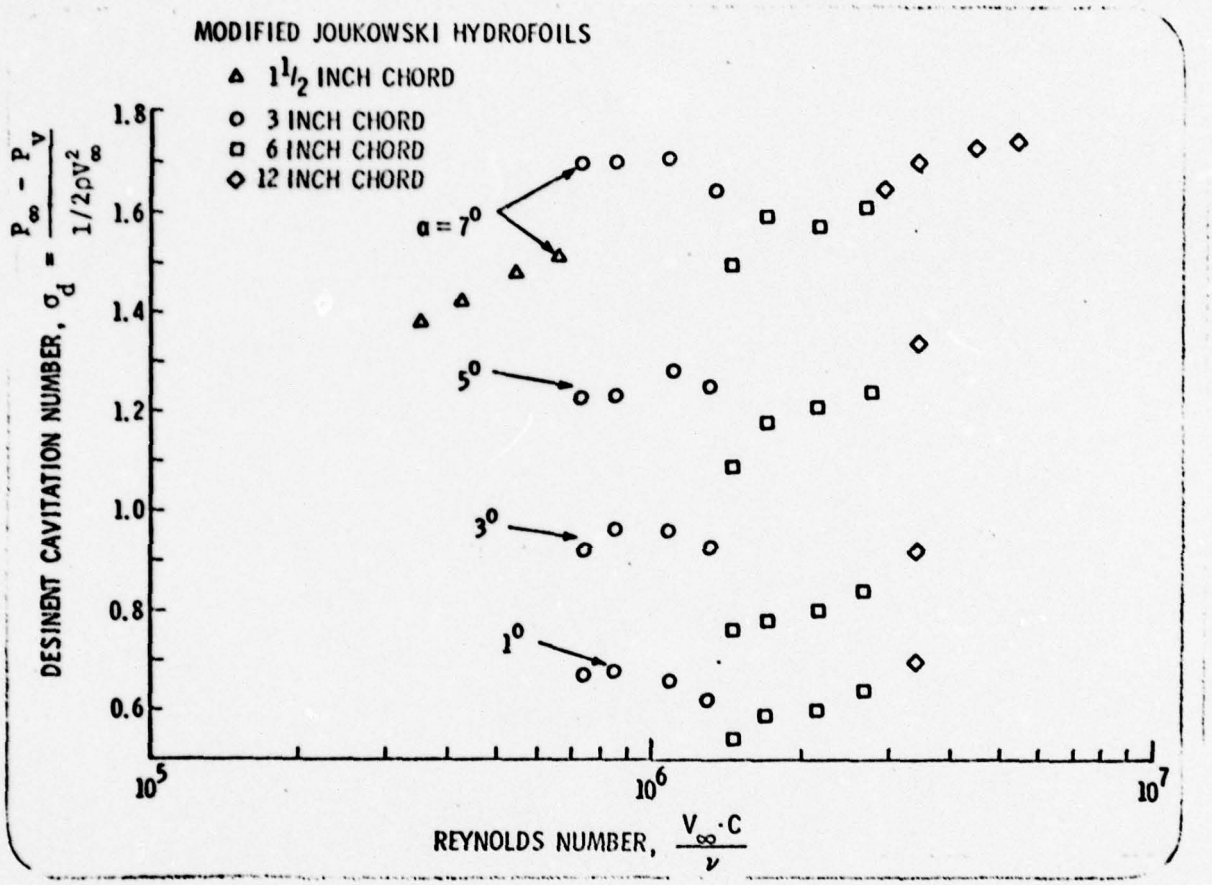

FIGURE 10 - Desinent Cavitation Number versus Reynolds Number for Hydrofoils at Various Angles of Attack.

December 16, 1977
DET;MLB:sk

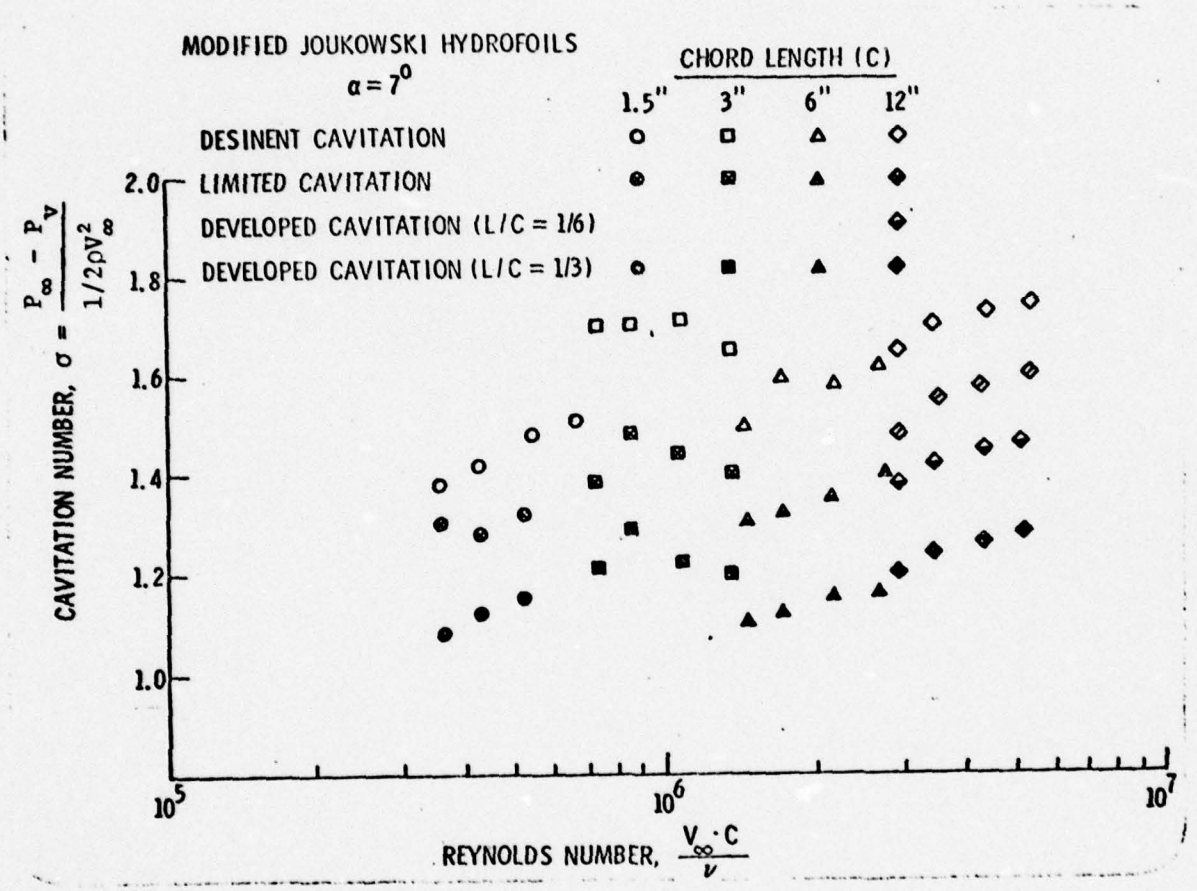

FIGURE 11 - Cavitation Number versus Reynolds Number for Various Cavitation States on Hydrofoils.

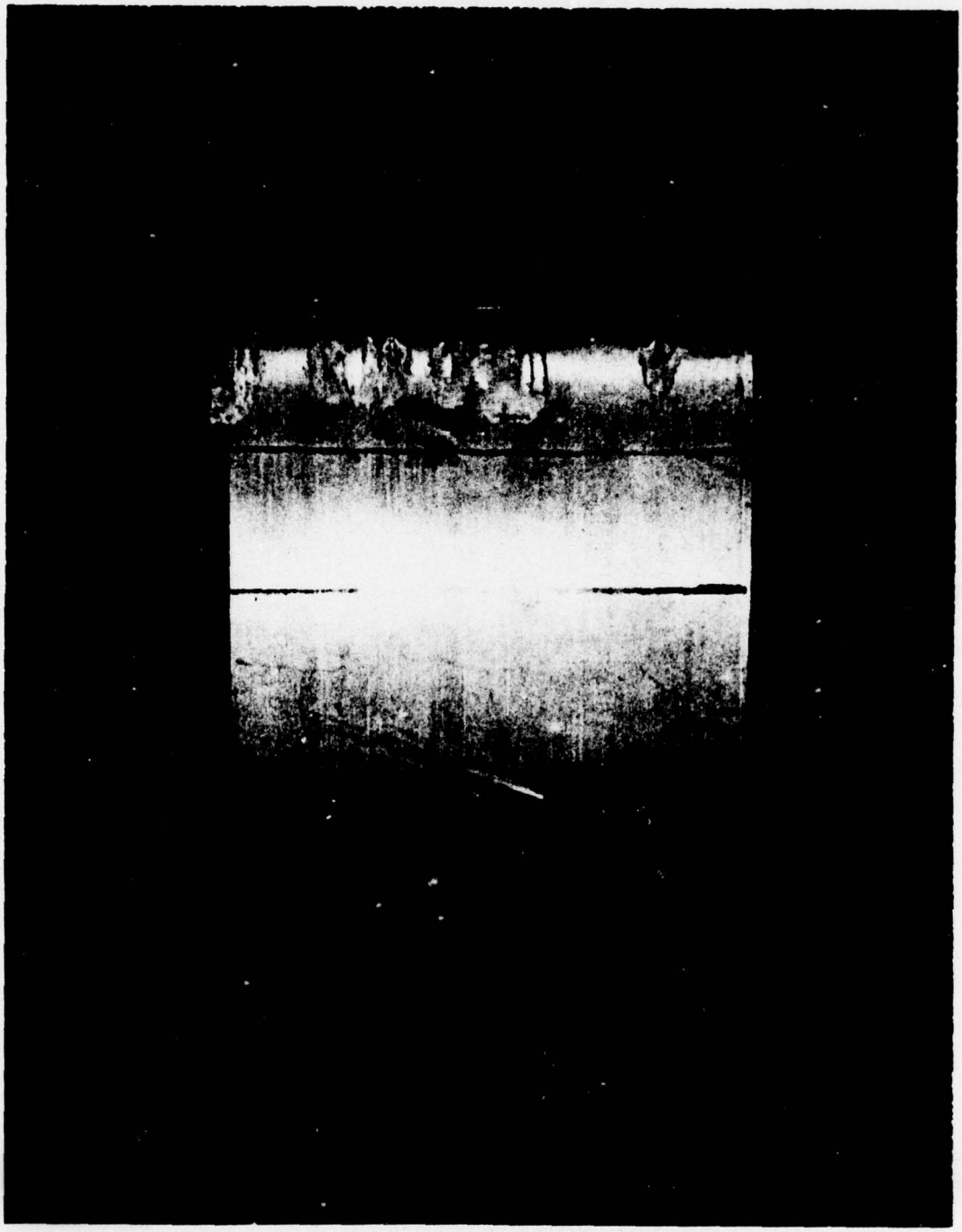

FIGURE 12 - Spotty Type Cavitation at 7^{o} Angle of Attack.
($C = 12"$, $V_{\infty} = 45fps$)

FIGURE 13 - Typical Developed Cavitation at 7^{o} Angle of Attack for L/C ≈ 1/6. (C = 12", V_{∞} = 45fps)

FIGURE 14 - Typical Developed Cavitation at 7° Angle of Attack for L/C = 1/3. (C = 12", V_∞ = 45fps)

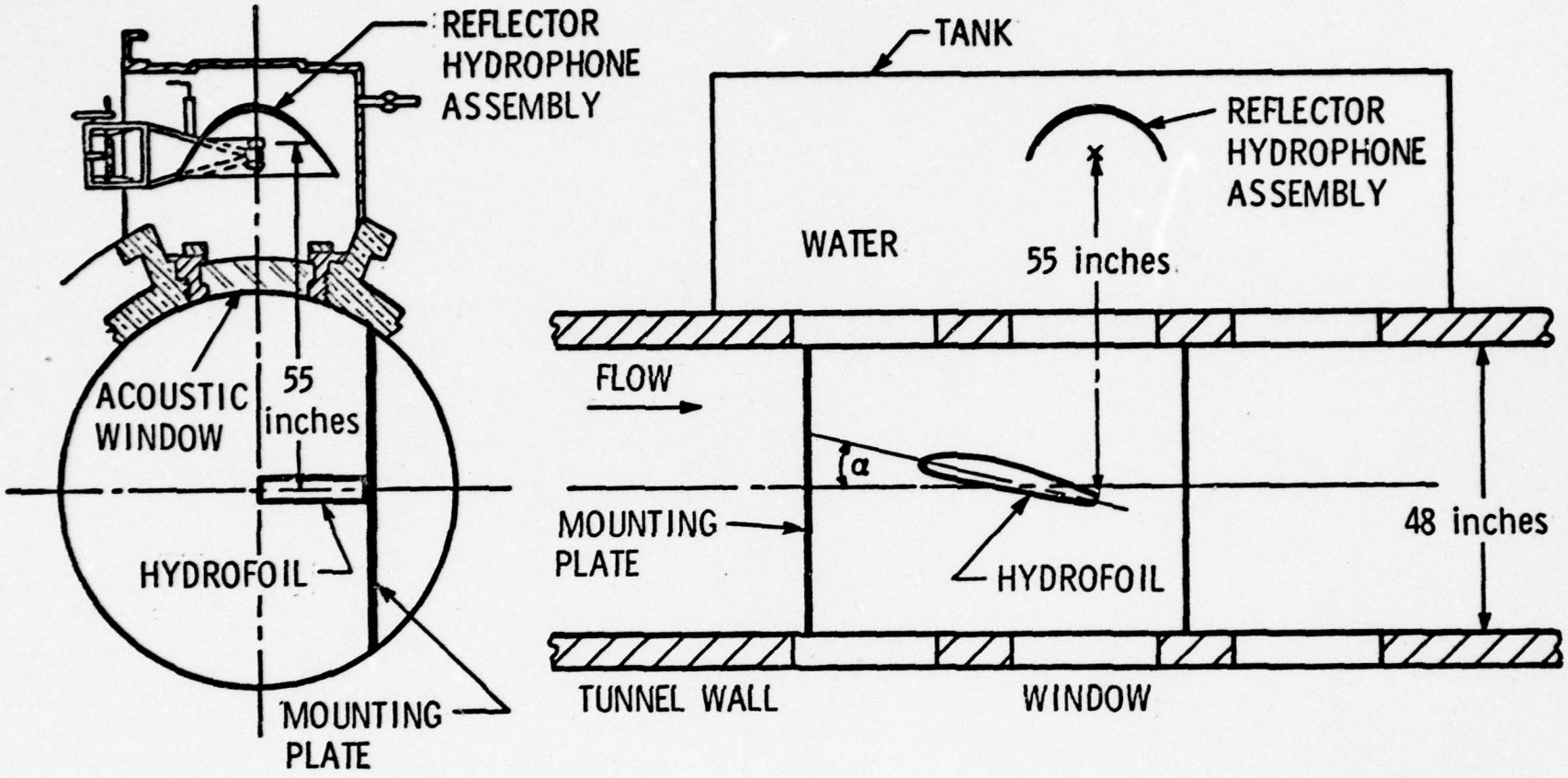

FIGURE 15 - Noise Measurement Apparatus.

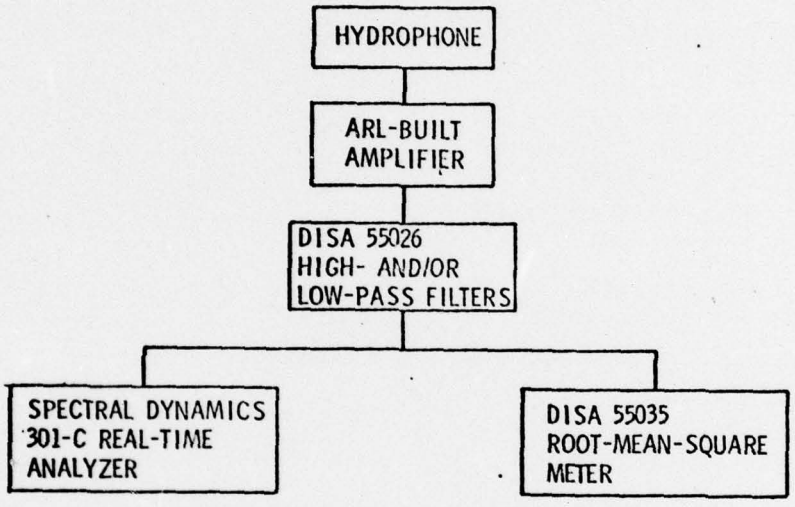

FIGURE 16 - Block Diagram of Data Acquisition and Analysis Equipment.

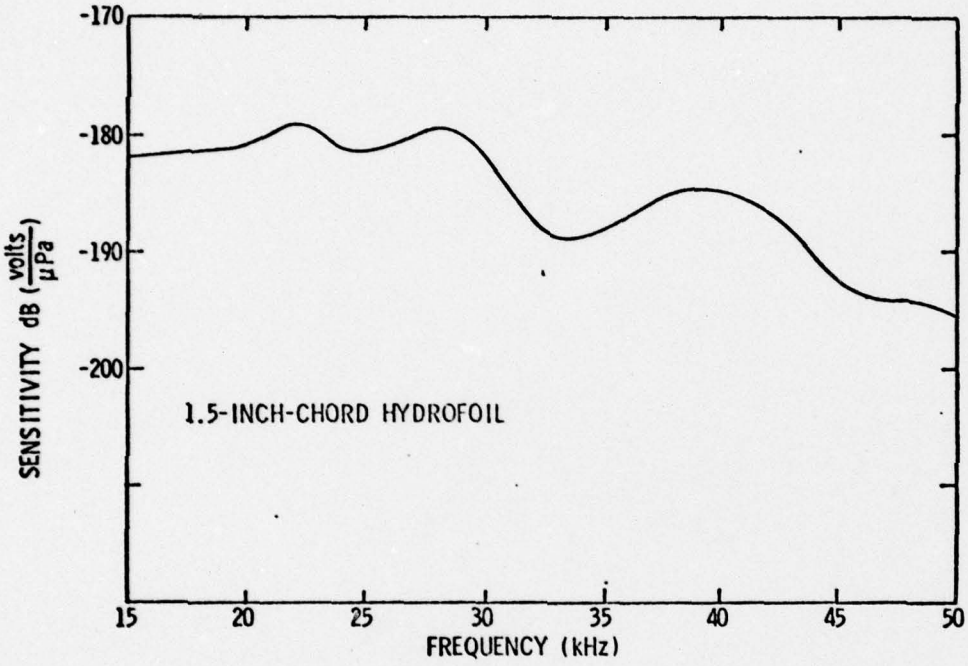

FIGURE 17 - Receiving Hydrophone Sensitivity for 1.5-inch Chord Hydrofoil.

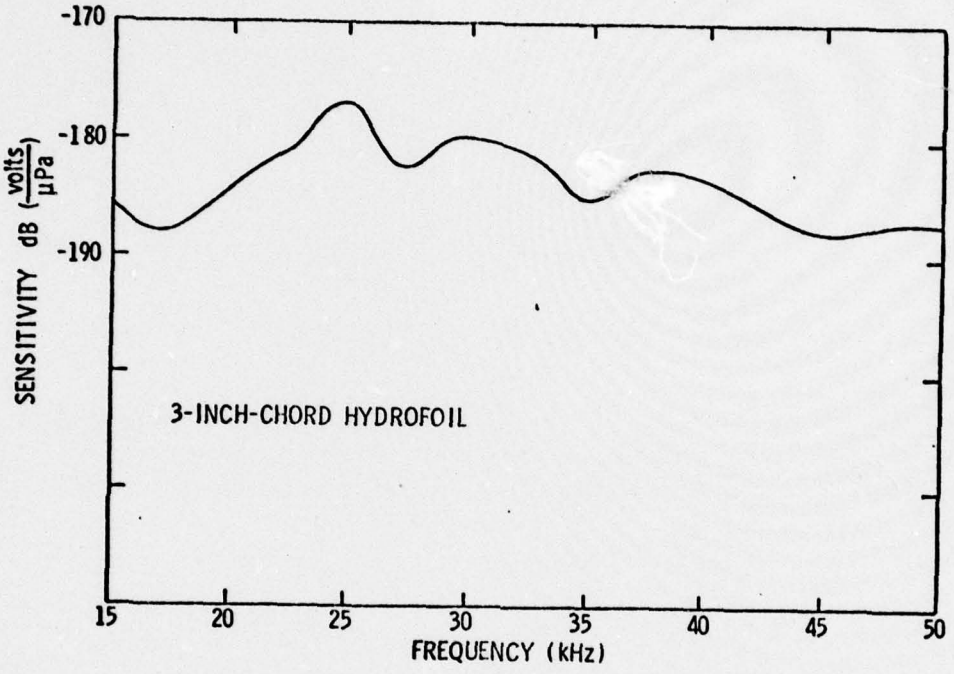

FIGURE 18 - Receiving Hydrophone Sensitivity for 3-inch Chord Hydrofoil.

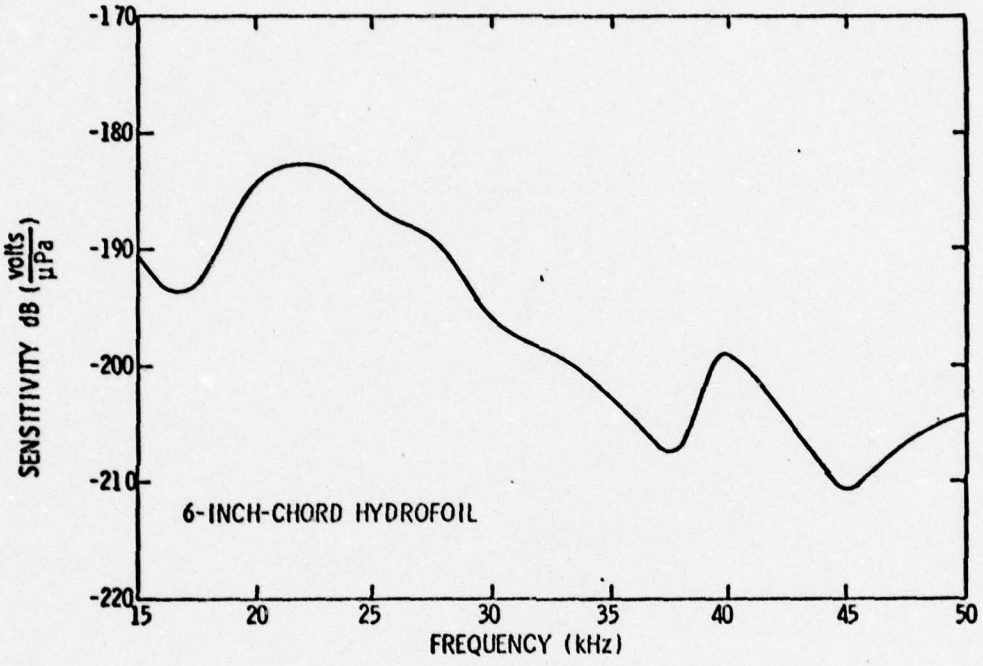

FIGURE 19 - Receiving Hydrophone Sensitivity for 6-inch Chord Hydrofoil.

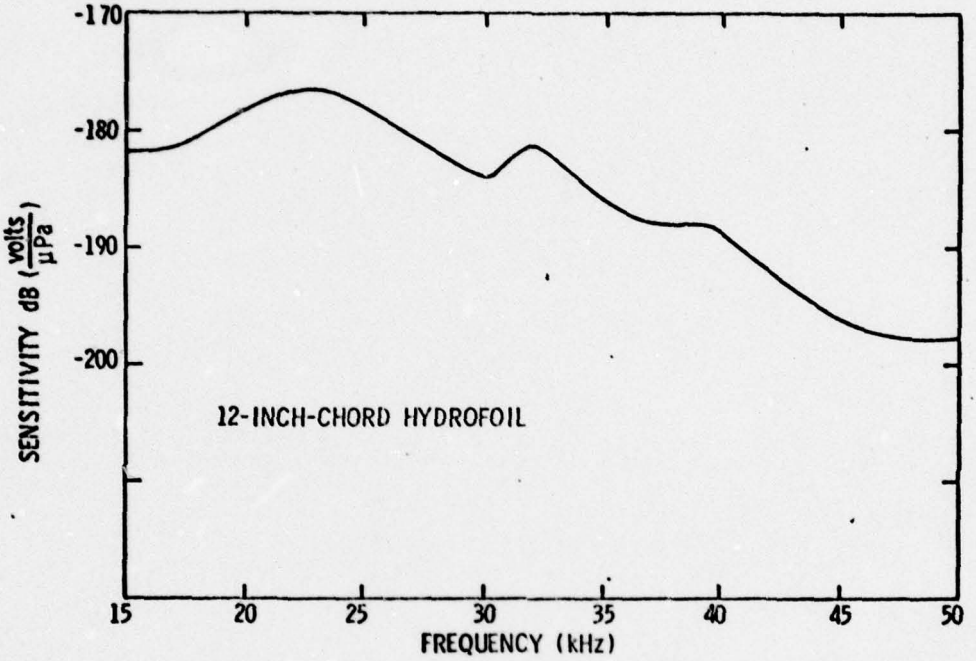

FIGURE 20 - Receiving Hydrophone Sensitivity for 12-inch Chord Hydrofoil.

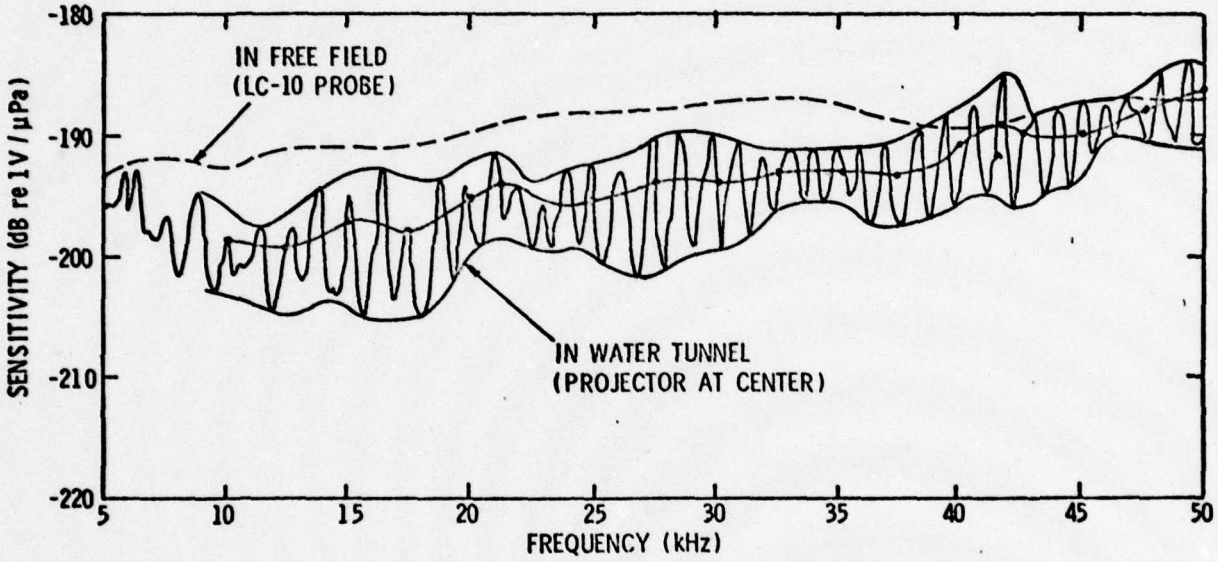

FIGURE 21 - Receiving Hydrophone Sensitivity in Free-Field and in Water Tunnel Setup.

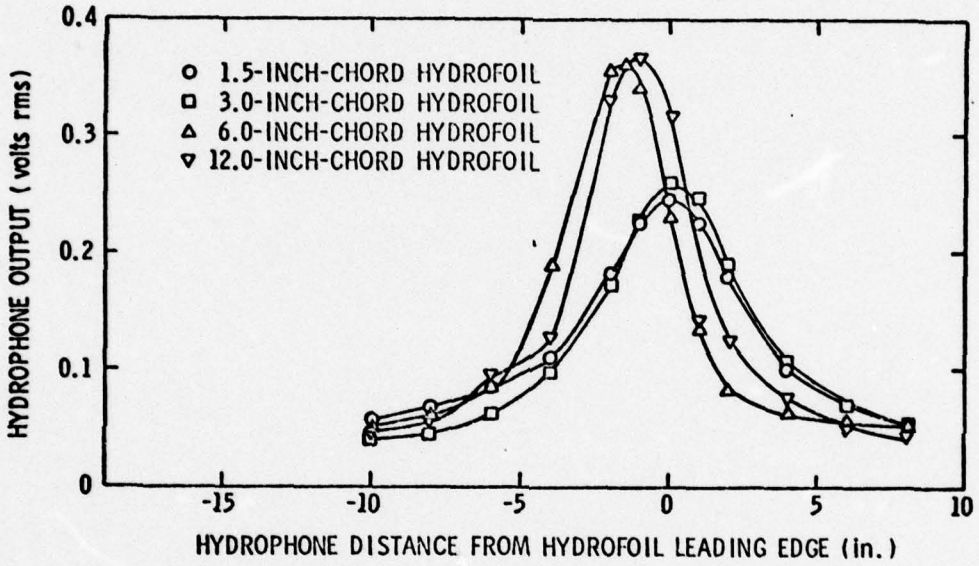

FIGURE 22 - Directivity with Each Hydrofoil Mounted in Test Section.

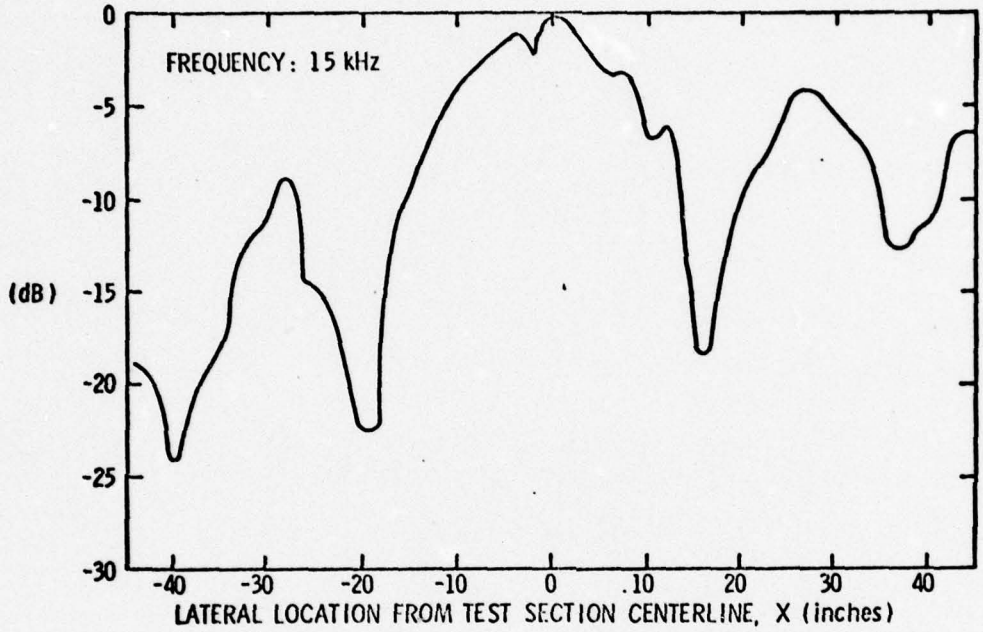

FIGURE 23 - Directivity in Water Tunnel without Model at 15kHz.

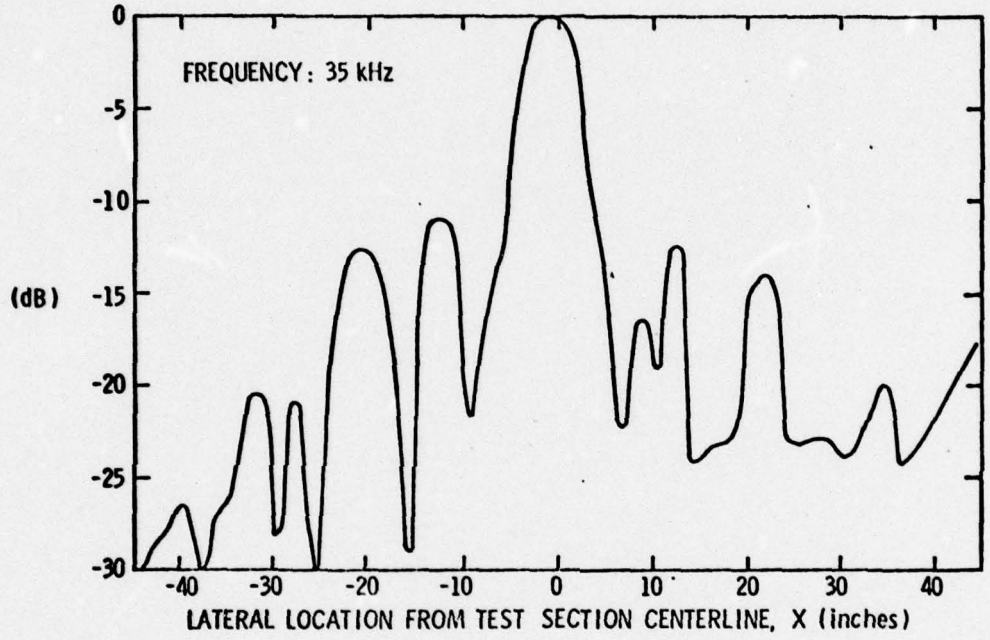

FIGURE 24 - Directivity in Water Tunnel without Model at 35kHz.

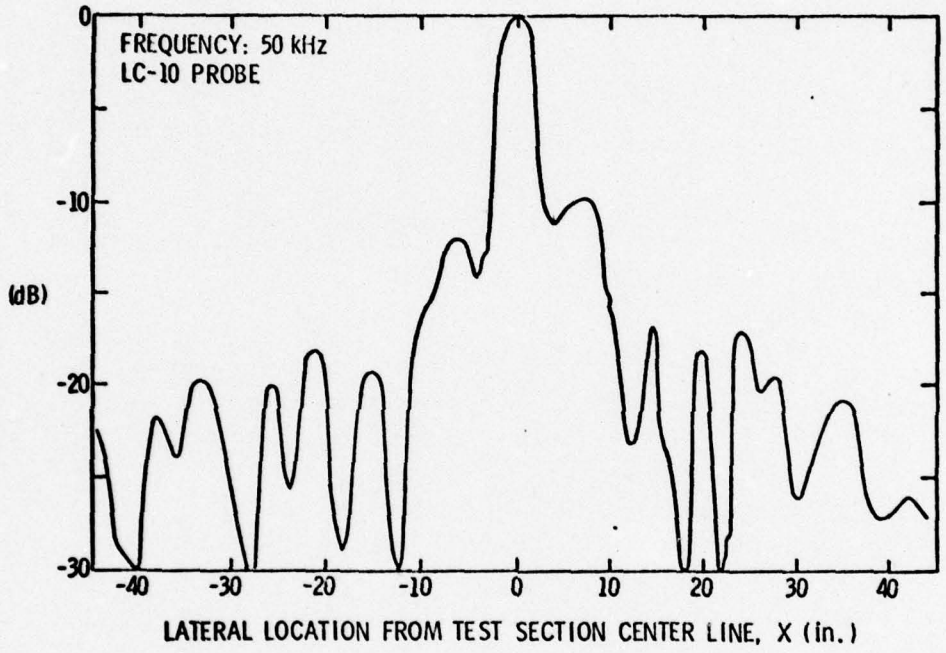

FIGURE 25 - Directivity in Water Tunnel without Model at 50kHz.

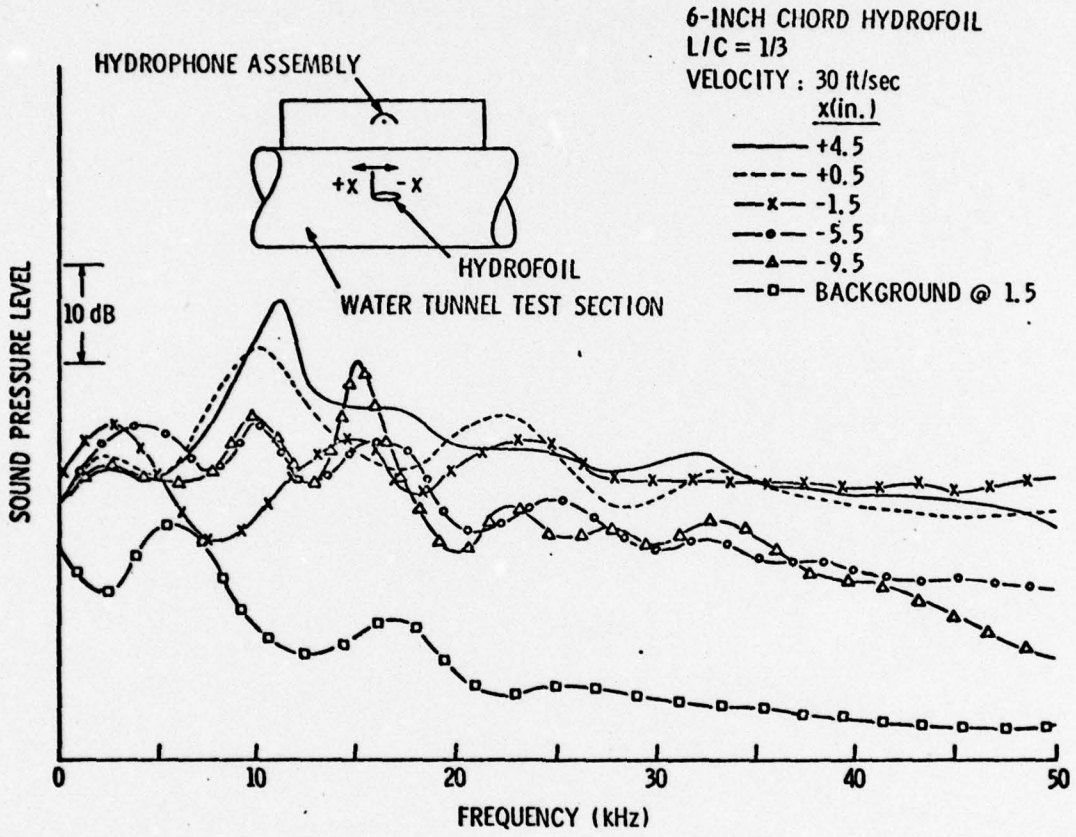

FIGURE 26 - Sound Pressure Level Spectra with Receiving Hydrophone at Various Axial Positions Relative to a Fixed Amount of Cavitation.

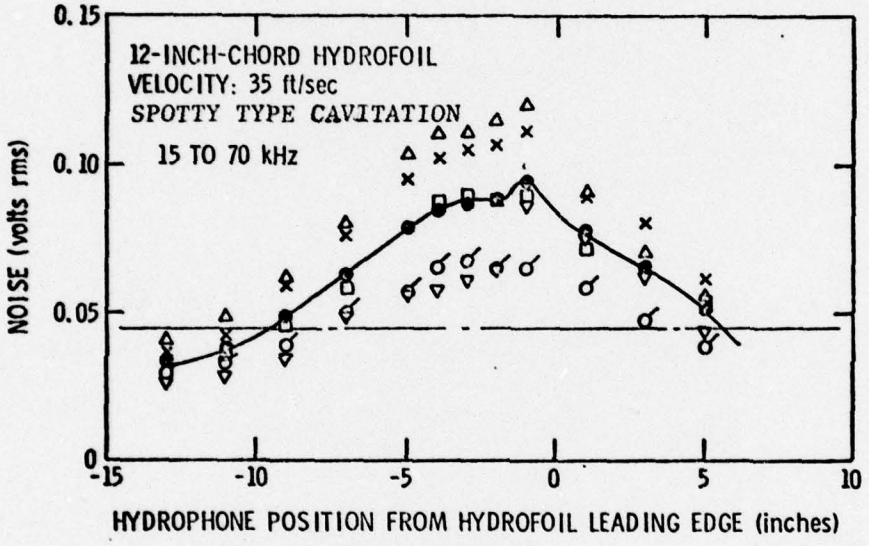

FIGURE 27 - RMS Noise Level versus Hydrophone Axial Position Depicting Noise Repeatability.

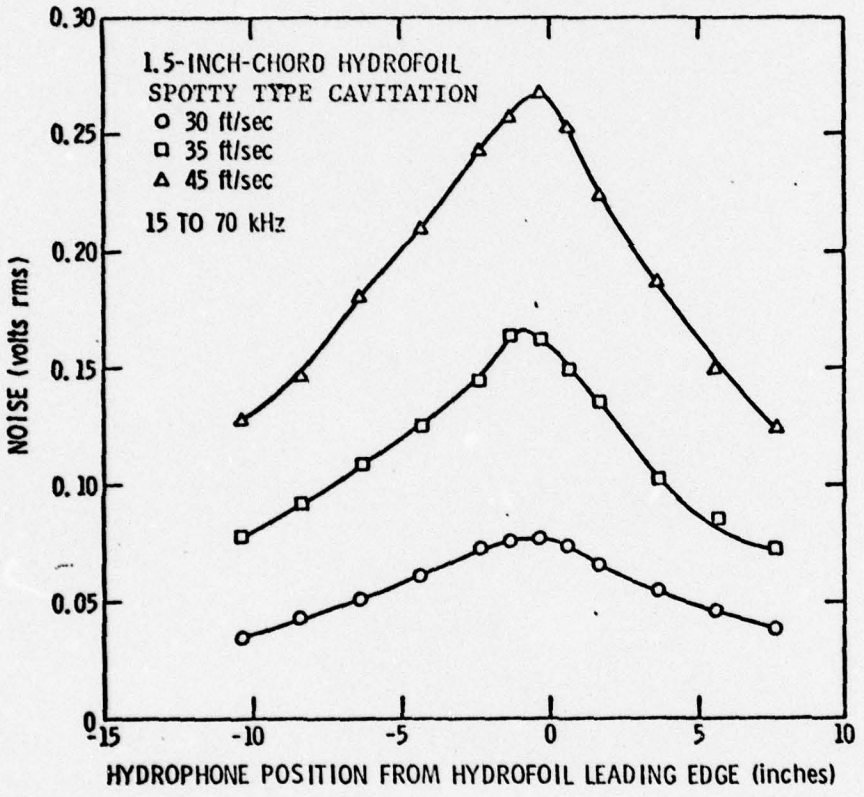

FIGURE 28 - RMS Noise Level versus Hydrophone Axial Position for 1.5-inch Chord Hydrofoil with Spotty Type Cavitation at Various Velocities.

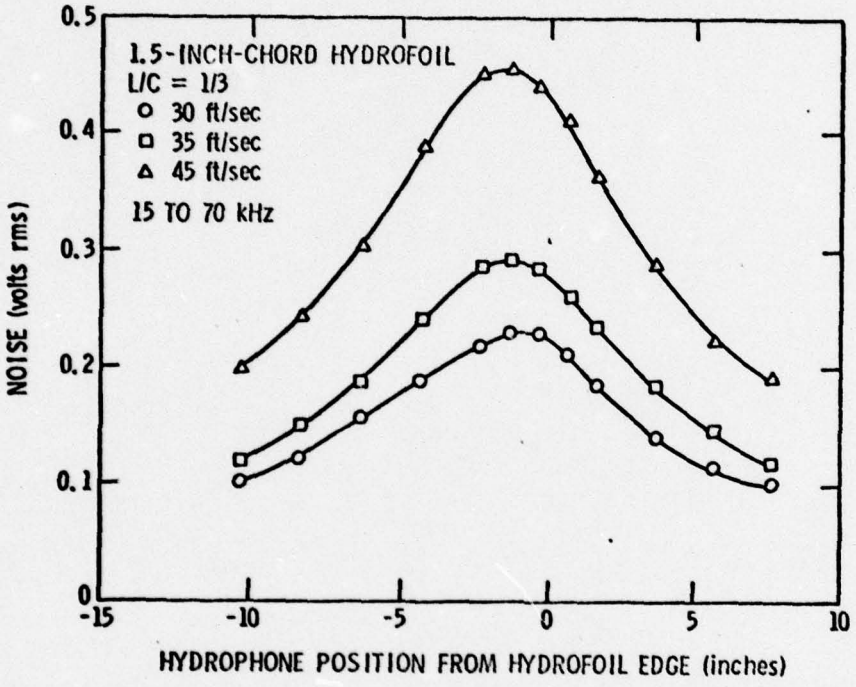

FIGURE 29 - RMS Noise Level versus Hydrophone Axial Position for 1.5-inch Chord Hydrofoil with L/C = 1/3 at Various Velocities.

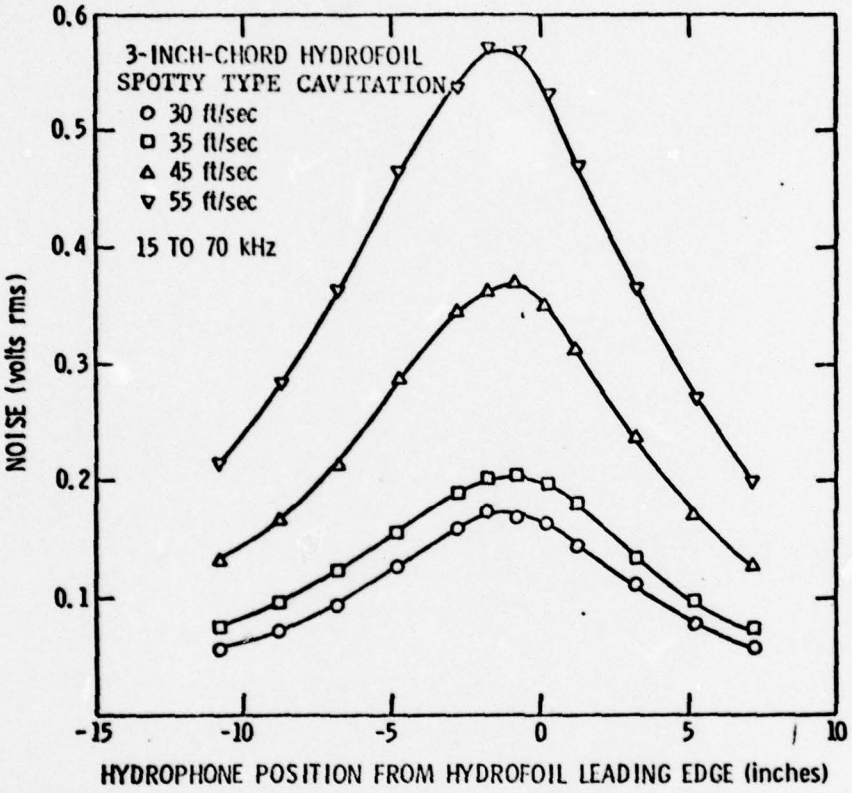

FIGURE 30 - RMS Noise Level versus Hydrophone Axial Position for 3-inch Chord Hydrofoil with Spotty Type Cavitation at Various Velocities.

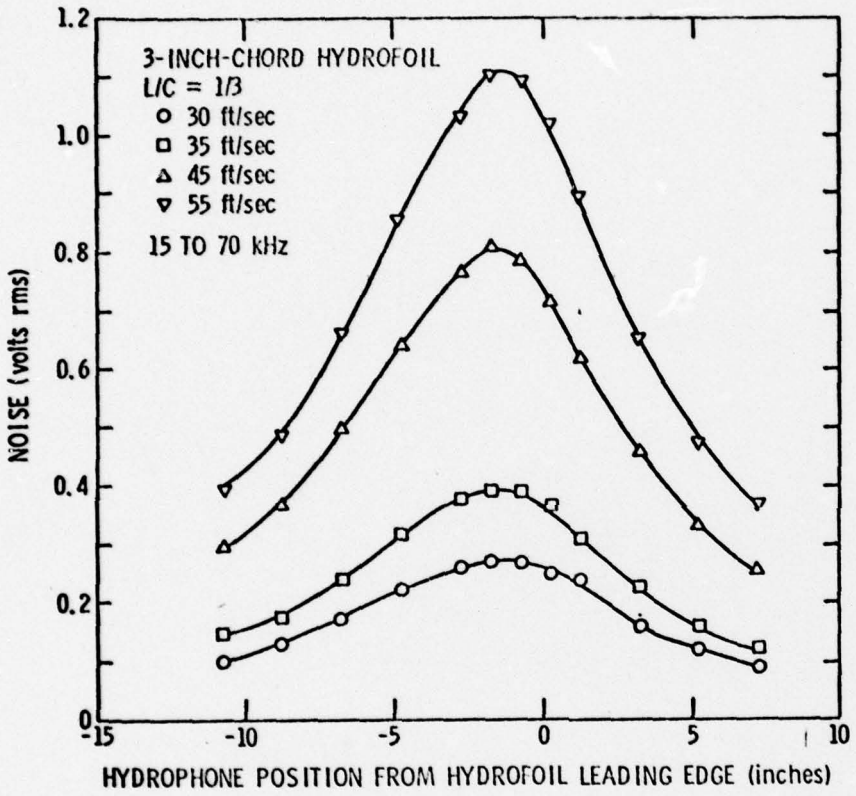

FIGURE 31 - RMS Noise Level versus Hydrophone Axial Position for 3-inch Chord Hydrofoil with L/C = 1/3 at Various Velocities.

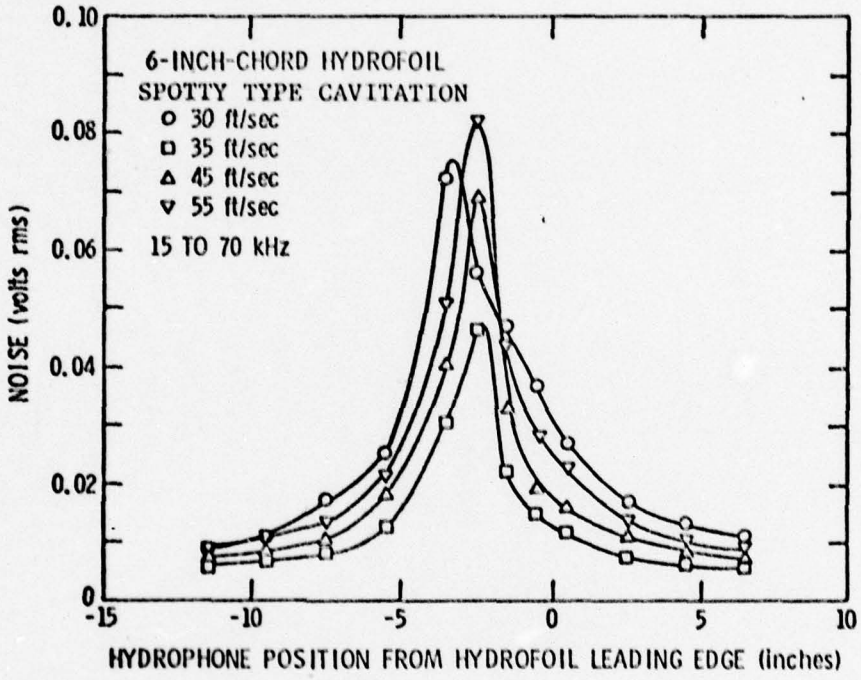

FIGURE 32 - RMS Noise Level versus Hydrophone Axial Position for 6-inch Chord Hydrofoil with Spotty Type Cavitation at Various Velocities.

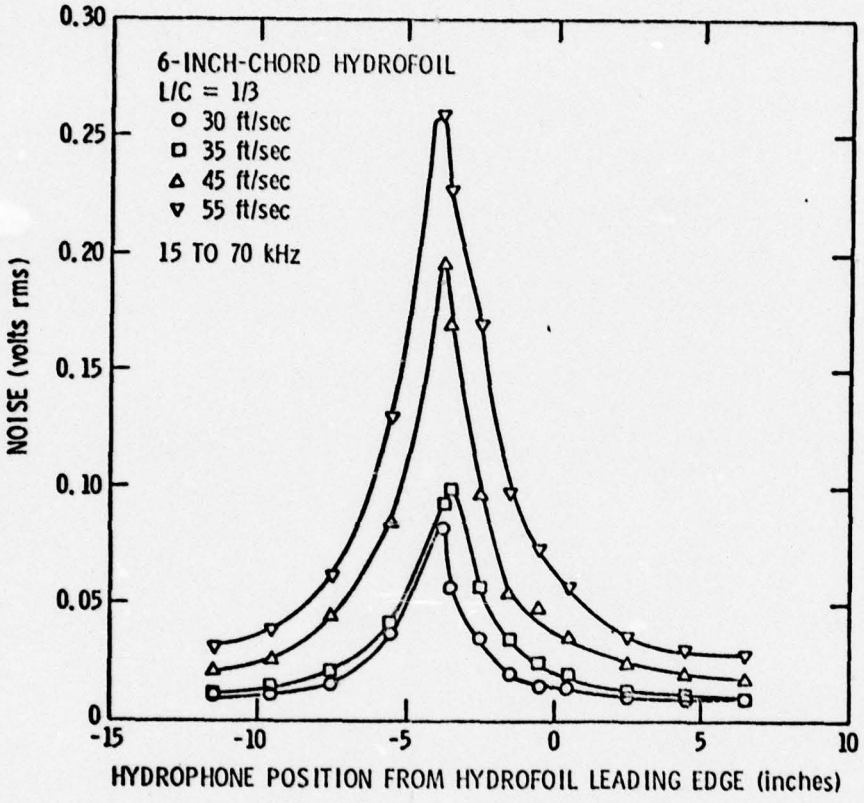

FIGURE 33 - RMS Noise Level versus Hydrophone Axial Position for 6-inch Chord Hydrofoil with L/C = 1/3 at Various Velocities.

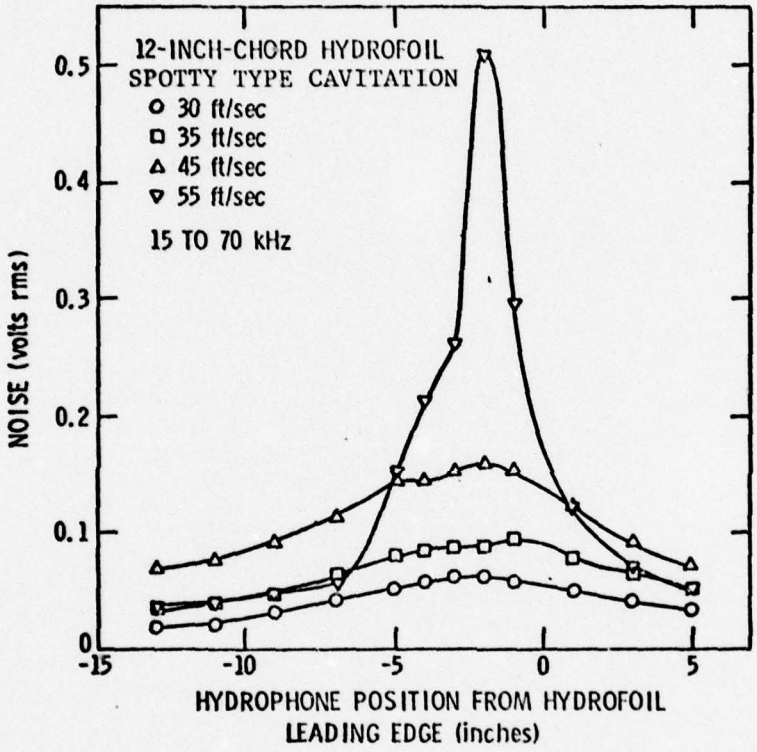

FIGURE 34 - RMS Noise Level versus Hydrophone Axial Position for 12-inch Chord Hydrofoil with Spotty Type Cavitation at Various Velocities.

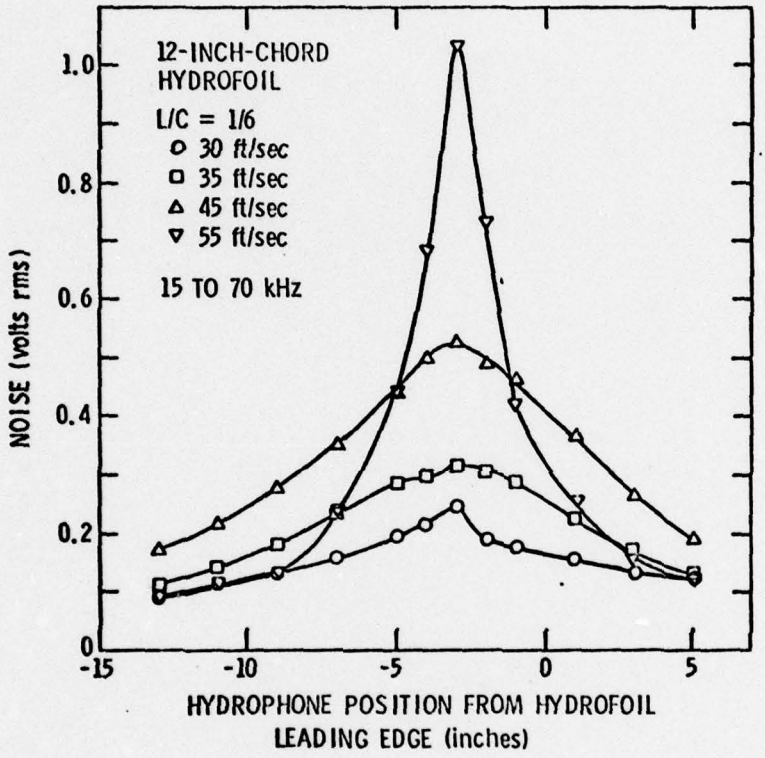

FIGURE 35 - RMS Noise Level versus Hydrophone Axial Position for 12-inch Chord Hydrofoil with L/C = 1/6 at Various Velocities.

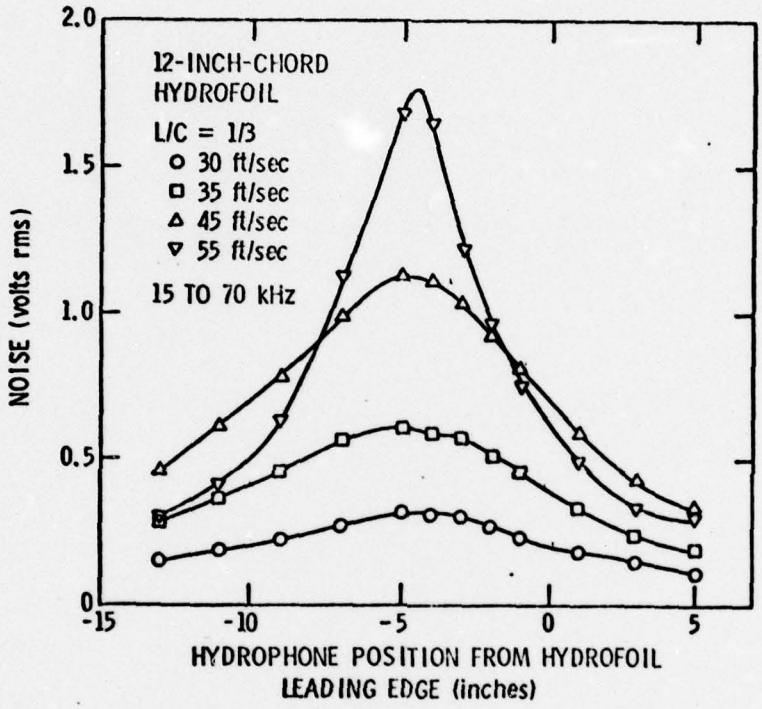

FIGURE 36 - RMS Noise Level versus Hydrophone Axial Position for 12-inch Chord Hydrofoil with L/C = 1/3 at Various Velocities.

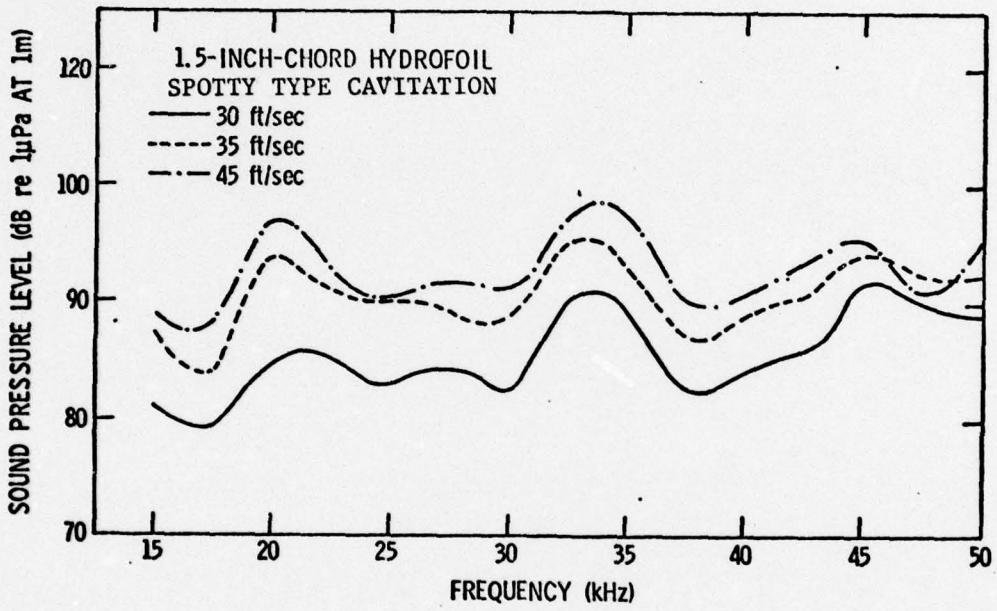

FIGURE 37 - Sound Pressure Level Spectra for 1.5-inch Chord Hydrofoil with Spotty Type Cavitation at Various Velocities.

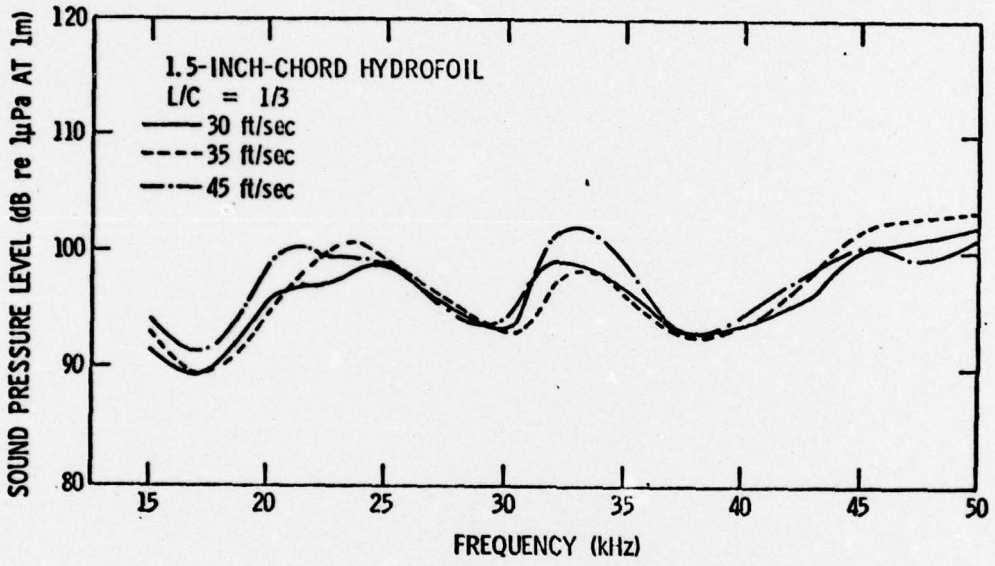

FIGURE 38 - Sound Pressure Level Spectra for 1.5-inch Chord Hydrofoil with L/C = 1/3 at Various Velocities.

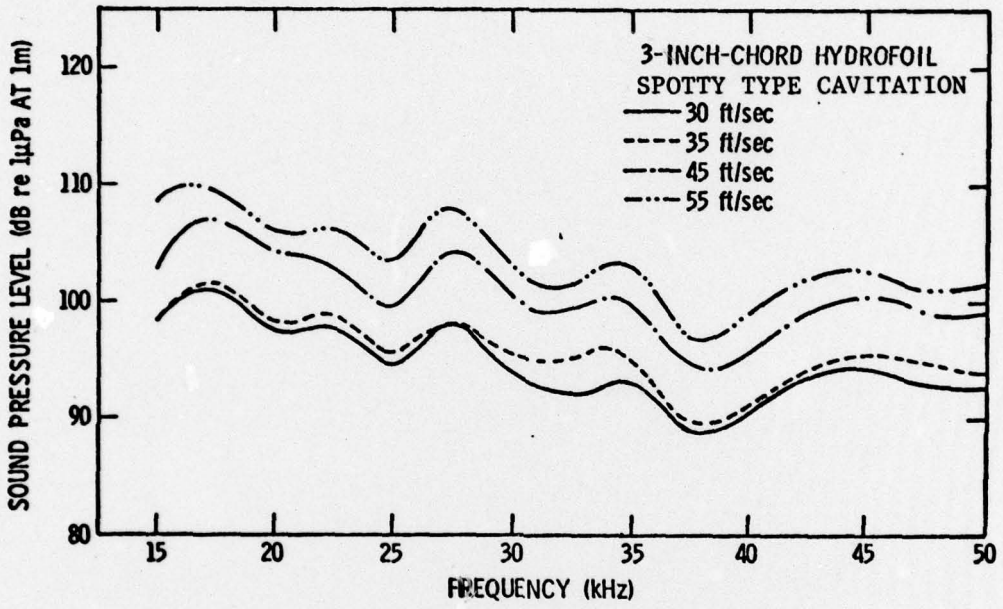

FIGURE 39 - Sound Pressure Level Spectra for 3-inch Chord Hydrofoil with Spotty Type Cavitation at Various Velocities.

December 16, 1977
DET;MLB:sk

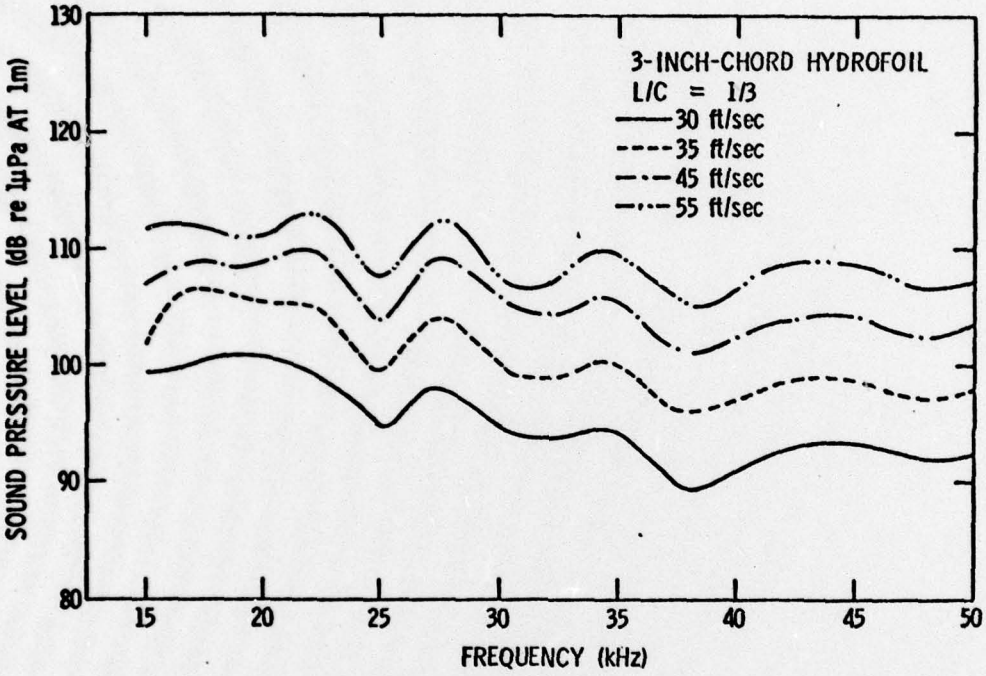

FIGURE 40 - Sound Pressure Level Spectra for 3-inch Chord Hydrofoil with L/C = 1/3 at Various Velocities.

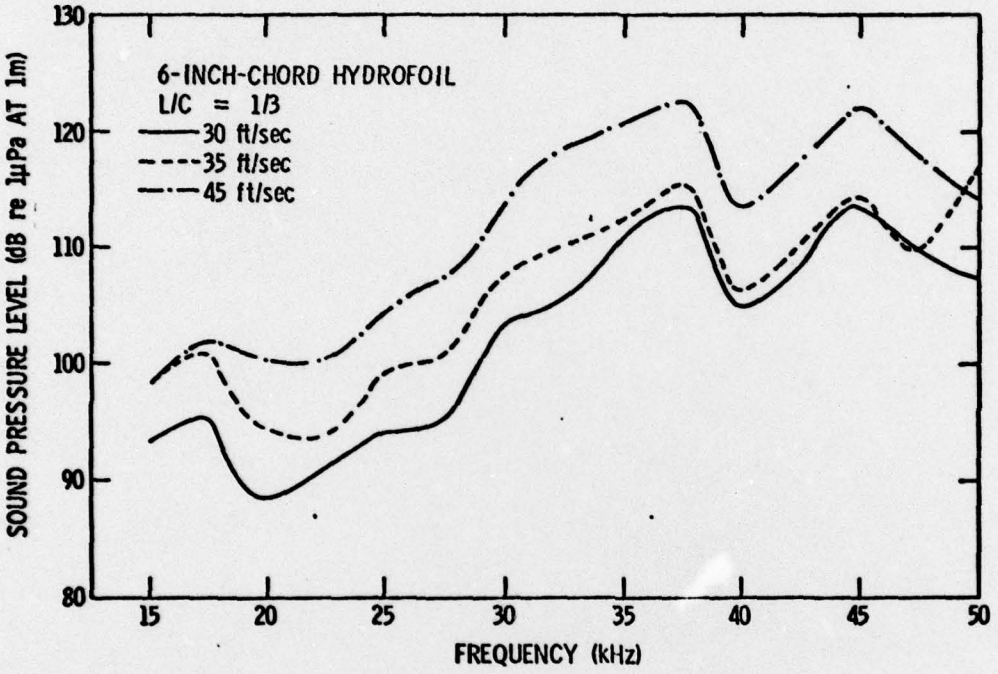

FIGURE 41 - Sound Pressure Level Spectra for 6-inch Chord Hydrofoil with L/C = 1/3 at Various Velocities.

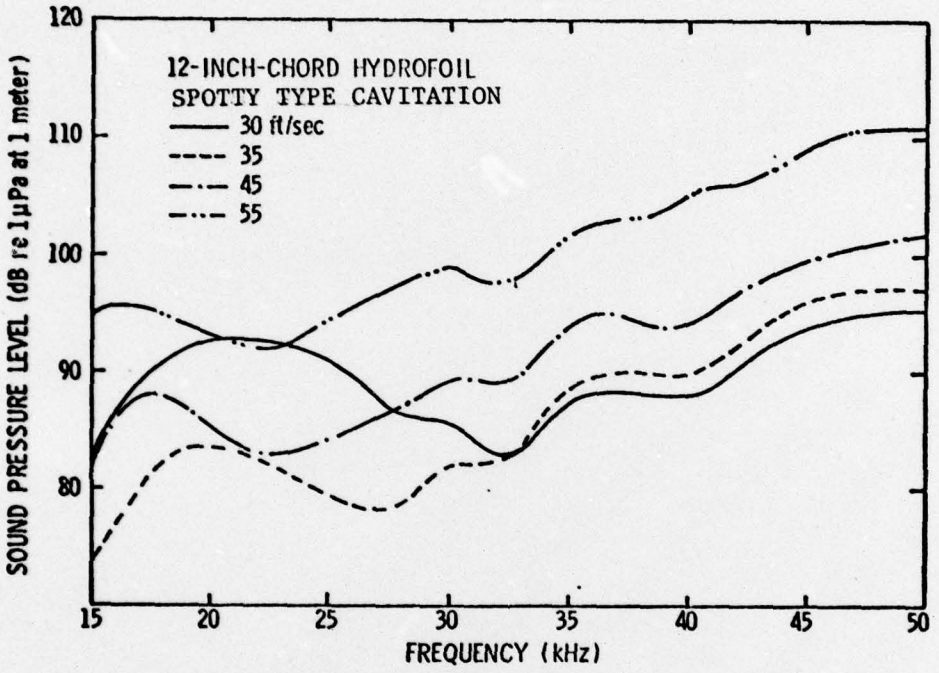

FIGURE 42 - Sound Pressure Level Spectra for 12-inch Chord Hydrofoil with Spotty Type Cavitation at Various Velocities.

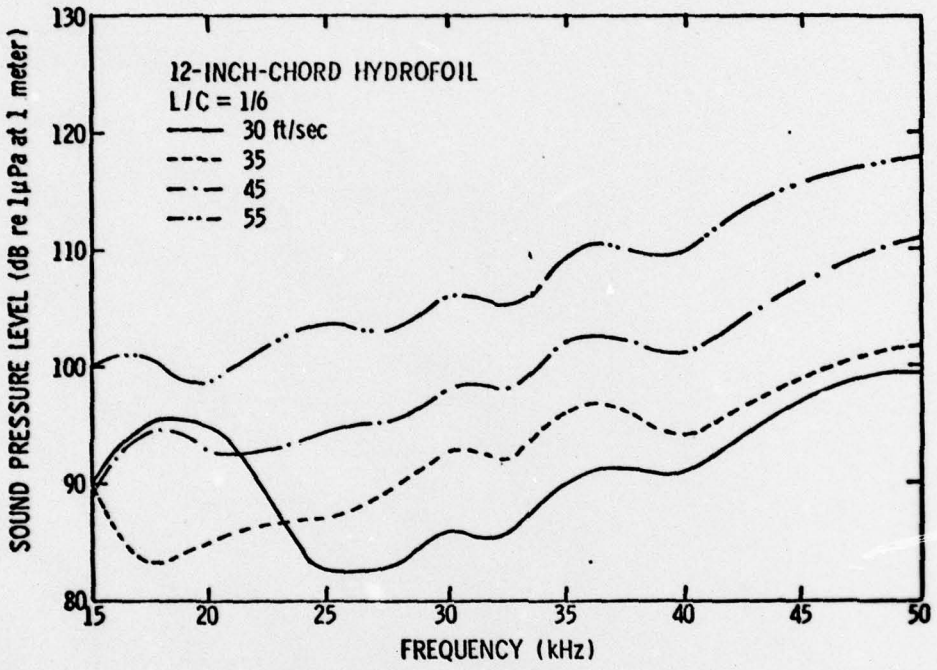

FIGURE 43 - Sound Pressure Level Spectra for 12-inch Chord Hydrofoil with L/C = 1/6 at Various Velocities.

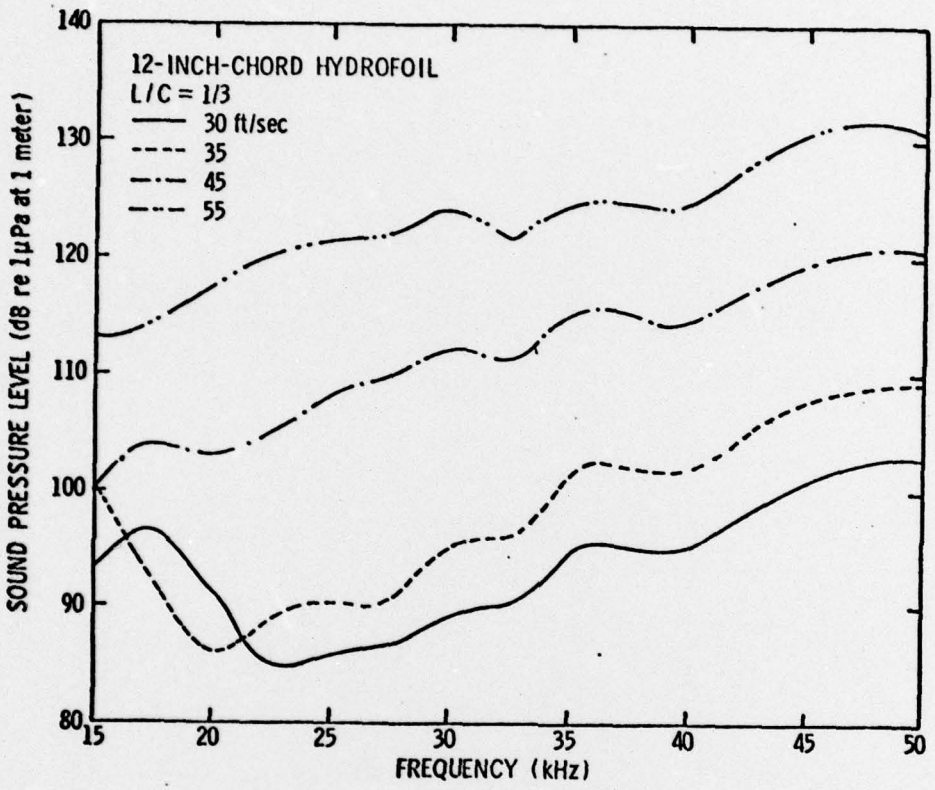

FIGURE 44 - Sound Pressure Level Spectra for 12-inch Chord Hydrofoil with L/C = 1/3 at Various Velocities.

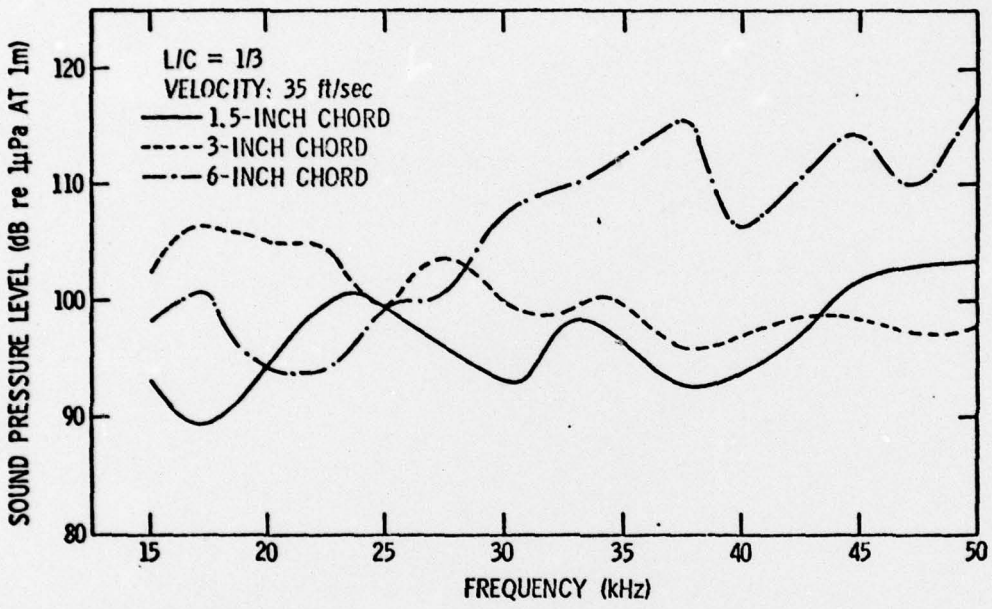

FIGURE 45 - Sound Pressure Level Spectra for Various Hydrofoils with L/C = 1/3 at a Velocity of 35 ft/sec.

December 16, 1977
DET;MLB:sk

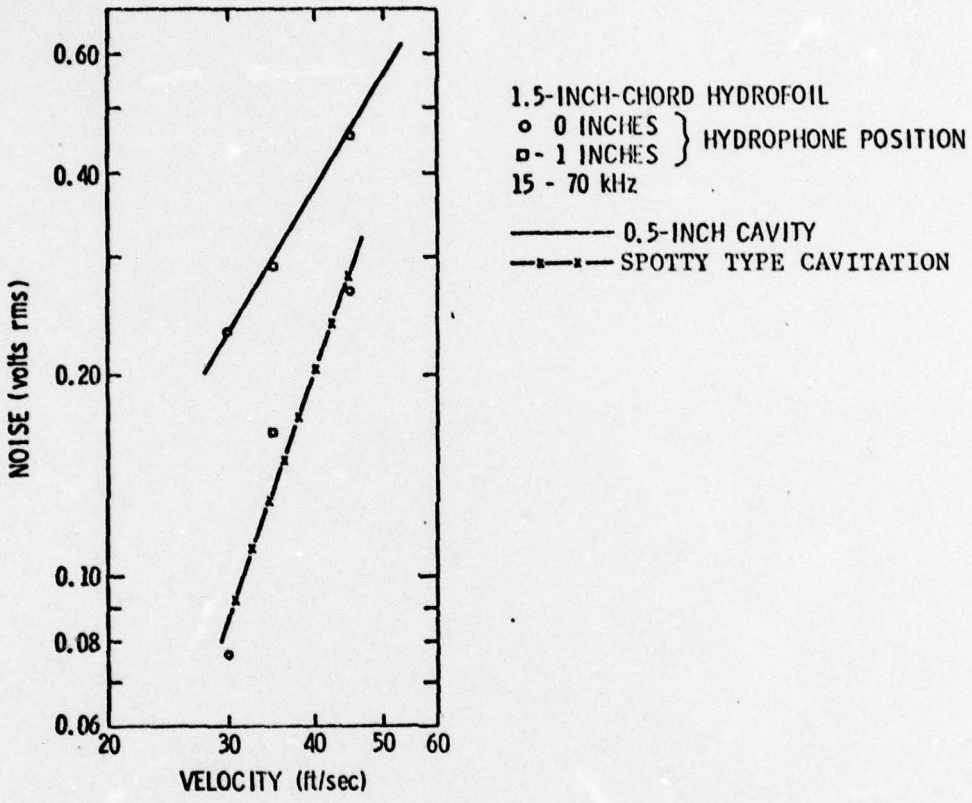

FIGURE 46 - RMS Noise Level versus Velocity for 1.5-inch Chord Hydrofoil with Spotty Type Cavitation and L/C = 1/3.

December 16, 1977
DET;MLB:sk

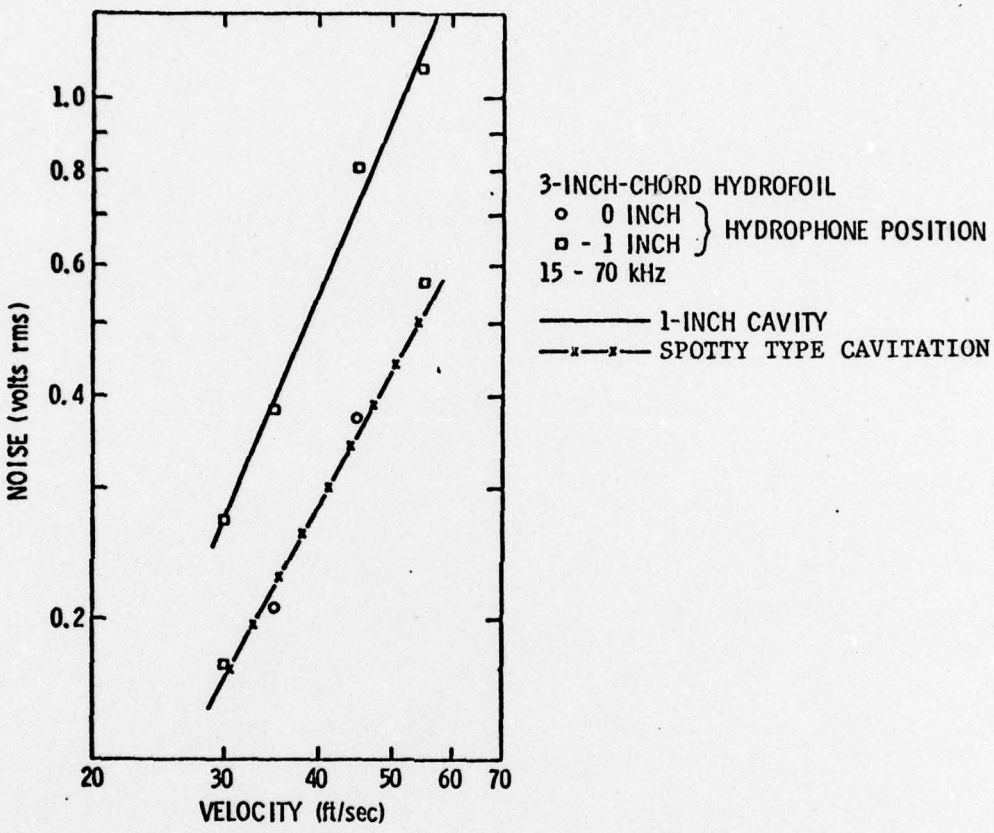

FIGURE 47 - RMS Noise Level versus Velocity for 3-inch Chord Hydrofoil with Spotty Type Cavitation and L/C = 1/3.

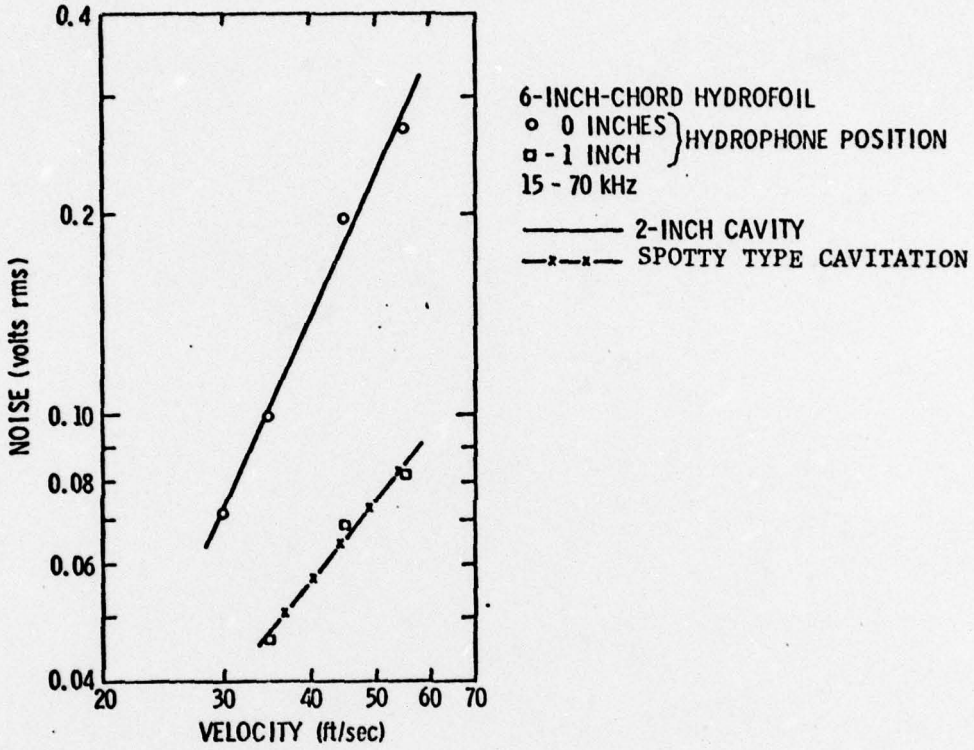

FIGURE 48 - RMS Noise Level versus Velocity for 6-inch Chord Hydrofoil with Spotty Type Cavitation and L/C = 1/3.

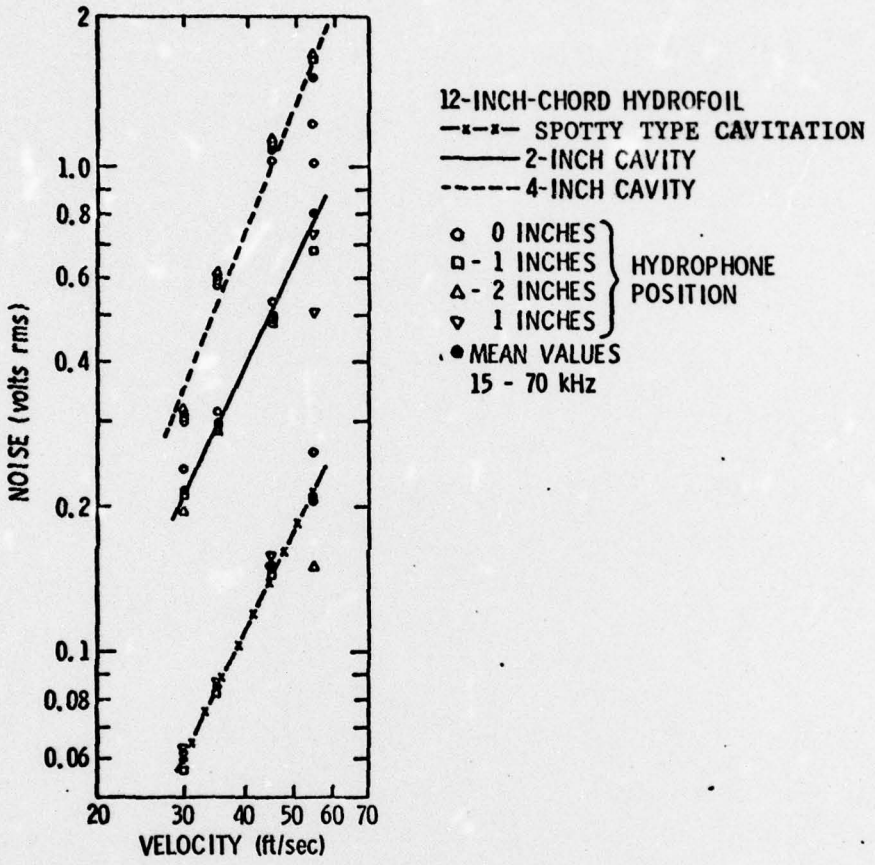

FIGURE 49 - RMS Noise Level versus Velocity for 12-inch Chord Hydrofoil with Spotty Type Cavitation, L/C = 1/6, L/C = 1/3.

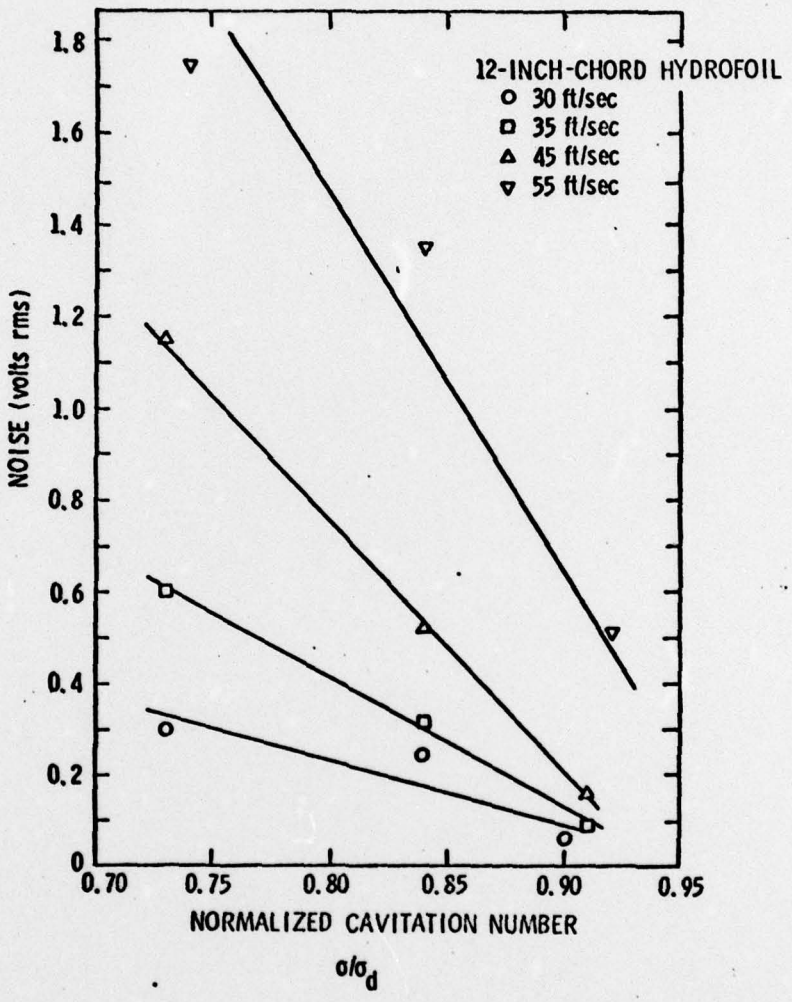

FIGURE 50 - RMS Noise Level versus Normalized Cavitation Number for the 12-inch Chord Hydrofoil with Various Velocities.

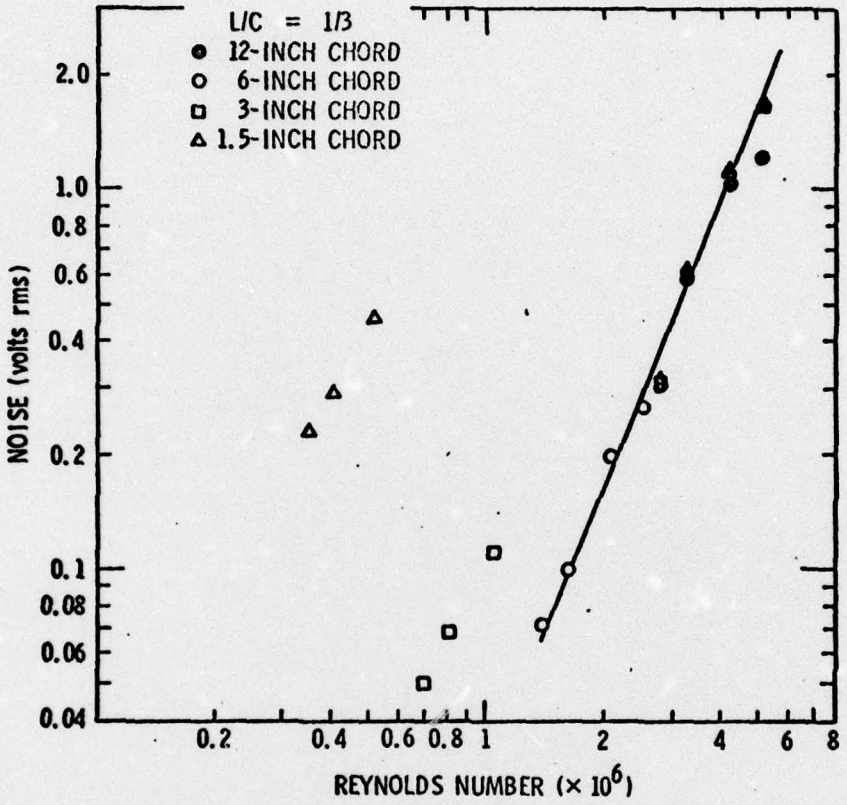

FIGURE 51 - RMS Noise Level versus Reynolds Number.